A Doctoral Dissertation

Effects of Oxidative Stress Induced by Silver Nanoparticles on Cell Death

Mei-Jing Piao

Department of Medicine

Graduate School

Jeju National University

February, 2012

은나노입자에 의한 산화적 스트레스가 세포사멸에 미치는 영향

지도교수 현 진 원

박 미 경

이 논문을 의학 박사학위 논문으로 제출함
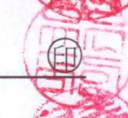
2012년 2월

박미경의 의학 박사학위 논문을 인준함

심사위원장 _____

위　　　원 _____

위　　　원 _____

위　　　원 _____

위　　　원 _____

제주대학교 대학원

2012년 2월

Effects of Oxidative Stress Induced by Silver Nanoparticles on Cell Death

Mei-Jing Piao

(Supervised by Professor Jin-Won Hyun)

A thesis submitted in partial fulfillment of the requirement for the degree of Doctor of Philosophy in Medicine

2012. 02

This thesis has been examined and approved.

DEOKBAE PARK

HEON JOO PARK

Eun Sook Yoo

Heekyoung Kang

Jin Won Hyun

2011. 12. 14

Department of Medicine

GRADUATE SCHOOL

JEJU NATIONAL UNIVERSITY

BACKGROUNDS

Silver nanoparticles (AgNPs) products, which have well-known antimicrobial properties, are extensively used as various medical and general products. Despite the widespread use of AgNPs products, relatively few studies have been undertaken to determine the cytotoxic effects of AgNPs exposure. This study investigates possible molecular mechanisms underlying the cytotoxic effects of AgNPs.

Initially, we show that AgNPs-induced cytotoxicity was higher compared to $AgNO_3$, as a silver ion source. AgNPs induced reactive oxygen species (ROS) generation via suppression of reduced glutathione (GSH) in human Chang liver cells. ROS generated by AgNPs resulted in damaged cellular components; DNA breaks, lipid membrane peroxidation, and protein carbonylation. Cell viability after AgNPs exposure was decreased via apoptosis, as shown by formation of apoptotic bodies, sub-G_1 hypodiploid cells, and DNA fragmentation. AgNPs induced a mitochondria-dependent apoptotic pathway via the modulation of Bax and Bcl-2 expressions, resulting in the disruption of mitochondrial membrane potential ($\Delta\psi_m$). Loss of the $\Delta\psi_m$ was followed by cytochrome c release from the mitochondria, resulting in the activation of caspase 9 and 3. The apoptotic effect of AgNPs was exerted via the activation of c-Jun NH2-terminal kinase (JNK) and was abrogated by the JNK specific inhibitor, SP600125, and small interfering RNA (siRNA) targeting JNK.

8-Oxoguanine (8-oxoG) is a sensitive marker of ROS-induced DNA damage. 8-Oxoguanine DNA glycosylase 1 (OGG1) is an important DNA repair enzyme that recognizes and excises 8-oxoG. The further study was to examine the effect of AgNPs-induced oxidative stress on OGG1 and to elucidate mechanisms underlying AgNPs-induced toxicity. AgNPs decreased OGG1 mRNA and protein expression, resulted in the attenuation of OGG1 activity, further led to increased 8-oxoG levels. The transcription factor NF-E2-

related factor 2 (Nrf2) is an important factor in the inducible regulation of OGG1. AgNPs treatment decreased nuclear Nrf2 expression, translocation into nucleus, and transcriptional activity. Extracellular regulated kinase (ERK) and protein kinase B (PKB, AKT), which are upstreams of Nrf2, contribute to OGG1 expression. AgNPs attenuated both active forms of ERK and AKT protein expression, resulting in suppression of Nrf2 and decrease of OGG1 expression.

Antioxidant enzymes such as catalase (CAT) and glutathione peroxidase (GPx) have been reported to directly protect the cells from oxidative stress. The final part of the study is to investigate the roles of antioxidants in the high intracellular levels of ROS induced by AgNPs in human Chang liver cells and the molecular mechanisms involved. AgNPs increased ROS levels, coincided with the decreased expressions and activities of CAT and GPx, and cell survival, but the addition of N-acetylcysteine (NAC), a potent antioxidant, significantly reduced the ROS levels, restored the activities of CAT and GPx, and finally abated cell deaths. AgNPs decreased an AMP-activated protein kinase (AMPK)-forkhead transcription factor 3 (FOXO3) pathway, which is a signal pathway for the induction of antioxidant enzymes. The AMPK activator (AICAR) significantly restored the expressions of CAT and GPx with the reduction of ROS levels and cytotoxicity, whereas the opposite changes were observed with an AMPK inhibitor (Compound C). In addition, knockdown of AMPK by its specific siRNA markedly enhanced ROS generation and cytotoxicity.

In conclusion, this study shows that AgNPs causes cytotoxicity by oxidative stress-induced apoptosis and damage of cellular components. Studies also demonstrate that down-regulation of Nrf2-mediated OGG1 in exposure to AgNPs occurs through ERK and AKT inactivation. AgNPs-induced oxidative cytotoxicity also might be at least partially attributed to the diminished antioxidant enzyme activities via the inhibition of the AMPK-FOXO3 pathway.

Keywords: Silver nanoparticles; oxidative stress; glutathione; apoptosis; 8-Oxoguanine DNA glycosylase 1; 8-Oxoguanine; NF-E2-related factor 2; Reactive oxygen species; Antioxidant enzyme; AMP-activated protein kinase; Forkhead transcription factor 3.

Abbreviations used: AgNPs, silver nanoparticles; ROS, reactive oxygen species; GSH, glutathione; $\Delta\psi_m$, mitochondrial membrane potential; JNK, c-Jun NH2-terminal kinase; HR-MAS NMR, high-resolution magic angle spinning nuclear magnetic resonance; TEM, transmission electron microscopy; DLS, dynamic light scattering; THF, tetrahydrofuran; MTT, [3-(4,5-dimethylthiazol-2-yl)-2,5-diphenyltetrazolium] bromide; DCF-DA, 2′,7′-dichlorodihydrofluorescein diacetate; PI, propidium iodide; GCLC, catalytically active subunit of glutamate-cysteine ligase; GSS, glutathione synthetase; JC-1, 5,5',6,6'-Tetrachloro-1,1',3,3'-tetraethylbenzimidazolylcarbocyanine iodide; CMAC, tert-butoxycarbonyl-Leu-Met-7-amino-4-chloromethylcoumarine; DPPP, diphenyl-1-pyrenylphosphine; SP600125, anthrax [1,9-cd] pyrazol-6(2H)-one; PBS, phosphate buffered saline; TSP, 3-(trimethylsilyl) propionic-2, 2, 3, 3-d_4 acid; LMA, low melting agarose; siRNA, small interfering RNA; NAC, N-acetyl cysteine; γ-GCL, γ-glutamate cystein ligase; 8-oxoG, 8-Oxoguanine; OGG1, 8-Oxoguanine DNA glycosylase 1; Nrf2, NF-E2-related factor 2; ERK, Extracellular regulated kinase; PKB or AKT, protein kinase B; CAT, catalase; GPx, glutathione peroxidase; AMPK, AMP-activated protein kinase; FOXO3, forkhead transcription factor 3; SOD, superoxide dismutase; AICAR, 5-aminoimidazole-4-carboxamide-1-β-D-ribofuranosyl 5′-monophosphate; ChIP, chromatin immunoprecipitation; RT-PCR, reverse transcription-polymerase chain reaction; BER, base excision repair; MAPK, mitogen activated protein kinase; TRITC, tetramethylrhodamine isothiocyanate.
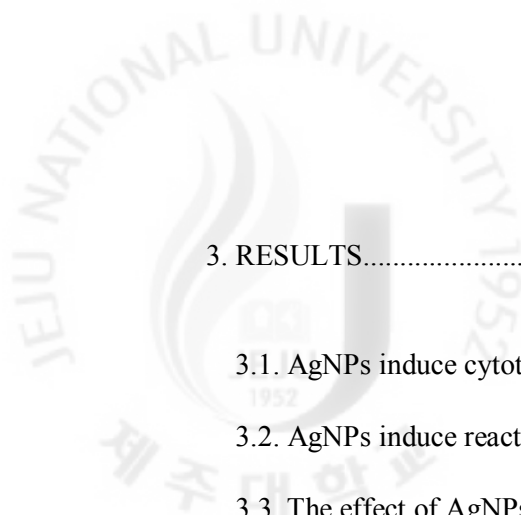
CONTENTS

PART ONE

2.1. Reagents

2.2. Cell culture

2.3. Cell viability

2.4. Observation by phase contrast inverted microscopy

2.5. Intracellular ROS measurement

2.6. Detection of reduced GSH level by using high-resolution magic angle spinning nuclear magnetic resonance (HR-MAS NMR) spectroscopy

2.7. Intracellular GSH measurement

2.8. Western blot analysis

2.9. Single cell gel electrophoresis (Comet assay)

2.10. Lipid peroxidation assay

2.11. Protein carbonyl formation

2.12. Nuclear staining with Hoechst 33342

2.13. Detection of apoptotic sub-G_1 hypodiploid cells

2.14. DNA fragmentation

2.15. $\Delta\psi_m$ analysis

2.16. Transient transfection of siRNA

2.17. Statistical analysis

PART TWO

PART THREE

LIST OF FIGURES

PART I

Silver nanoparticles induce oxidative cell damage in human liver cells through inhibition of reduced glutathione and induction of mitochondria-involved apoptosis

ABSTRACT

AgNPs products, which have well-known antimicrobial properties, are extensively used as various medical and general products.

Despite the widespread use of AgNPs products, relatively few studies have been undertaken to determine the cytotoxic effects of AgNPs exposure. This study investigates possible molecular mechanisms underlying the cytotoxic effects of AgNPs. Here, we show that AgNPs-induced cytotoxicity was higher compared to $AgNO_3$, as a silver ion source. AgNPs induced ROS generation via suppression of reduced GSH in human Chang liver cells. ROS generated by AgNPs resulted in damaged cellular components; DNA breaks, lipid membrane peroxidation, and protein carbonylation. Cell viability after AgNPs exposure decreased via apoptosis, as shown by formation of apoptotic bodies, sub-G_1 hypodiploid cells, and DNA fragmentation. AgNPs induced a mitochondria-dependent apoptotic pathway via the modulation of Bax and Bcl-2 expressions, resulting in the disruption of $\Delta\psi_m$. Loss of the $\Delta\psi_m$ was followed by cytochrome c release from the mitochondria, resulting in the activation of caspase 9 and 3. The apoptotic effect of AgNPs was exerted via the activation of JNK and was abrogated by the JNK specific inhibitor, SP600125, and siRNA targeting JNK. In summary, the results suggest that AgNPs causes cytotoxicity by oxidative stress-induced apoptosis and damage of cellular components.

Keywords: Silver nanoparticles; oxidative stress; glutathione; apoptosis.

1. INTRODUCTION

Nanoparticles range in length from 1 to 100 nm in two or three dimensions (Lewinski et al., 2008). Nanoparticles are used in bioapplications as therapeutics, transfection vectors, and fluorescent labels (Kreuter and Gelperina, 2008; Su et al., 2008; Tan et al., 2007; Yoon et al., 2007). AgNPs are one of the most commonly used nanomaterials. For example, AgNPs are used in coating or embedding for medical purposes (Cohen et al., 2007; Fu et al., 2006; Xu et al., 2008). In addition to their medical uses, AgNPs are also used in clothing, the food industry, paints, electronics and other fields (Cheng et al., 2004; Cohen et al., 2007; Lee et al., 2007; Vigneshwaran et al., 2007). Despite their widespread use, there is a serious lack of information concerning the toxicity of AgNPs to humans and their underlying cellular actions. Recent studies have shown that AgNPs accumulation in the liver could induce cytotoxicity via oxidative cell damage (Hussain et al., 2005; Hsin et al., 2008; Kim et al., 2009).

ROS are continually generated and eliminated in biological systems. They play important roles in a variety of normal biochemical functions, and abnormality in their functions results in pathological processes. Excessive production of ROS in the cell is known to induce apoptosis (Martindale and Holbrook, 2002; Sastre et al., 2000). ROS generation has been shown to play an important role in apoptosis induced by treatment with AgNPs (Carlson et al., 2008; AshaRani et al., 2009; Foldbjerg et al., 2009). The JNK is a member of the mitogen-activated protein (MAP) kinase family and plays a proapoptotic function in response to various cellular stresses (Shen and Liu, 2006). JNK is strongly activated by ROS or by amild oxidative shift of the intracellular thiol/disulfide redox state, leading to apoptosis (Hsin et al., 2008; Mao et al., 2008). Although a few research groups have investigated the toxicity of AgNPs in terms of cell death via ROS generation, little is known about the mechanisms of AgNPs-mediated toxicity (Arora et al., 2008; Hussain et al., 2005). Our results suggest that AgNPs increase the
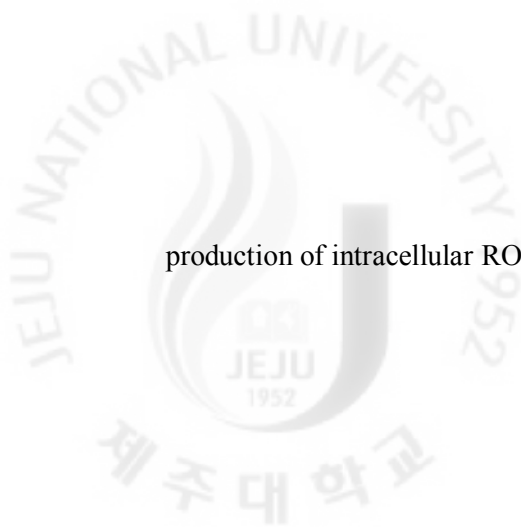
production of intracellular ROS and decrease reduced glutathione levels, leading to apoptosis.

2. MATERIALS AND METHODS

2.1. Reagents

Characterization of AgNPs was conducted as described previously (Eom and Choi, 2010). Energy filtering transmission electron microscopy (TEM) was used to examine the shape and size of the AgNPs. Twenty microliter of particle suspension was dried onto a 400 mesh carbon-coated copper grid and imaged using a LIBRA 120 TEM (Carl Zeiss, Oberkochen, Baden-Wurttemberg, Germany) at 80-120 kV. The size distribution of the AgNPs was evaluated using a photal dynamic light scattering (DLS) spectrometer (DLS-7000, Otsuka Electronics Co., Inc., Osaka, Japan). The particle size provided by the manufacturer was below 100nm (Sigma-Aldrich Chemical Company, St. Louis, MO, USA), however, the TEM images indicated that AgNPs prepared via the tetrahydrofuran (THF) method had an even distribution, with individual particle sizes ranging from 5 to 10 nm. AgNPs tend to agglomerate when exposed to cells; the results obtained by DLS indicated that the most of the NPs in the medium were of about 28-35nm in size. Ag ions were estimated using a multitype inductively coupled plasma emission spectrometer (ICPE-9000, Shimadzu, Tokyo, Japan). The concentrations of AgNPs and Ag ions had equivalent Ag masses and measured prior to exposure of the compounds to cell culture media. [3-(4,5-dimethylthiazol-2-yl)-2,5-diphenyltetrazolium] bromide (MTT), 2',7'-dichlorodihydrofluorescein diacetate (DCF-DA), propidium iodide (PI), and Hoechst 33342 were purchased from the Sigma-Aldrich Chemical Company. A catalytically active subunit of glutamate-cysteine ligase (GCLC) was purchased from Thermo Scientific (Fremont, CA, USA). Reduced glutathione synthetase (GSS) and siRNA against JNK were purchased from Santa Cruz Biotechnology (Santa Cruz, CA, USA). The primary anti-Bcl-2, -Bax, -cytochrome c, -caspase 9, -caspase 3, -phospho JNK, and -JNK antibodies were purchased from Cell Signaling Technology (Beverly, MA, USA). 5,5',6,6'-Tetrachloro-1,1',3,3'-

tetraethylbenzimidazolylcarbocyanine iodide (JC-1) was purchased from Invitrogen (Carlsbad, CA, USA). Tert-butoxycarbonyl-Leu-Met-7-amino-4-chloromethylcoumarine (CMAC) and diphenyl-1-pyrenylphosphine (DPPP) were purchased from Molecular Probe (Eugene, OR, USA). Anthrax [1,9-cd] pyrazol-6(2H)-one (SP600125) was purchased from Calbiochem (San Diego, CA, USA). All other chemicals and reagents were of analytical grade.

2.2. Cell culture

Human Chang liver cells were obtained from the American Type Culture Collection (Rockville, MD, USA) and maintained at 37 ℃ in an incubator with a humidified atmosphere of 5% CO_2 and cultured in RPMI-1640 medium containing 10% heat-inactivated fetal calf serum, streptomycin (100 μg/ml) and penicillin (100 U/ml).

2.3. Cell viability

Cells were treated with AgNPs and $AgNO_3$ at various concentrations. Twenty four hours later, 50 μl of the MTT stock solution (2 mg/ml) was added to each well for a total reaction volume of 200 μl. After incubating for 4 h, the plate was centrifuged at 800×g for 5 min followed by aspiration of the supernatants. The formazan crystals in each well were dissolved in 150 μl of dimethylsulfoxide and the A_{540} was read in a scanning multi-well spectrophotometer (Carmichael et al., 1987). To determine the effect of the JNK pathway on cell viability, cells were pre-treated with SP600125 (an inhibitor of JNK) for 1 h at a final concentration of 10 μM, followed by 4 μg/ml of AgNPs for 24 h. Cell viability was measured using the MTT assay.

2.4. Observation by phase contrast inverted microscopy

Cells were exposed to AgNPs for 24 h, washed with phosphate buffered saline (PBS), and

observed by phase contrast inverted microscopy at 100× magnification.

2.5. Intracellular ROS measurement

Cells were treated with AgNPs and incubated for various times at 37 ℃. After addition of 25 μM of DCF-DA, the fluorescence of 2',7'-dichlorofluorescein was detected using a Perkin Elmer LS-5B spectrofluorometer and a flow cytometer (Becton Dickinson, Mountain View, CA, USA) (Rosenkranz et al., 1992). The image analysis for the generation of intracellular ROS was achieved by seeding the cells on a cover-slip-loaded six well plate at $2×10^5$ cells/well. Sixteen hours after plating, the cells were treated with AgNPs. Thirty minutes later, 100 μM of DCF-DA was added to each well and was incubated for an additional 30 min at 37 ℃. After washing with PBS, the stained cells were mounted onto a microscope slide in mounting medium (DAKO, Carpinteria, CA, USA). The microscopic images were collected using the Laser Scanning Microscope 5 PASCAL program (Carl Zeiss, Jena, Germany) on a confocal microscope.

2.6. Detection of reduced GSH level by using high-resolution magic angle spinning nuclear magnetic resonance (HR-MAS NMR) spectroscopy

Twenty mg of cell pellet was loaded into a nano zirconium rotor. Deuterium oxide and TSP-d_4 were used as the field-lock frequency and chemical shift reference, respectively. The total volume was adjusted to 45 μl with deuterium oxide in 20 μl of deuterium oxide mixed with 5 μl of 20 mM 3-(trimethylsilyl) propionic-2, 2, 3, 3-d_4 acid (TSP) and was transferred into a 4 mm zirconium rotor (Chan et al., 2009). The rotor lid was closed and marked to monitor the spinning speed. Measurement of ^{1}H NMR spectra was carried out on a 400 MHz Varian Unity-Inova (Varian Inc., Palo Alto, CA, USA) operating at a proton frequency of 400.266 MHz. All instruments were equipped with HX nanoprobes with a spin rate of 2000 Hz and were

regulated at 147 ℃. The water signal was suppressed by a pre-saturation pulse sequence. Each ^{1}H NMR spectrum was recorded over 512 scans requiring about a 40 min total acquisition time. The acquisition time and relaxation delay time were 2 s and 1 s, respectively. All data were referenced to TSP-d$_4$ at δ 0.00 ppm and were apodized with an exponential function using a line broadening of 0.2 Hz. All NMR spectra were Fourier transformed, phased, and baseline corrected using MestreNova Suite 5.3.1. A spectral assignment was performed by ChenomX NMR Suite 6.01 software (ChenomX Inc., Canada). Spectra were normalized to the TSP concentration, superimposed, and stacked to compare GSH concentration.

2.7. Intracellular GSH measurement

Intracellular GSH content was measured using a commercial colorimetric assay kit, GSH-400 from OXIS International (Portland, OR, USA). Cells were harvested and were homogenized in ametaphosphoric working solution. After centrifugation, 50 μl of R1 solution (a solution of a chromogenic reagent in HCl) was added to 900 μl of supernatant, followed by gentle vortex mixing. Following the addition of 50 μl of R2 solution (30% NaOH), the mixtures were incubated at 25±3℃ for 10 min. After centrifugation, the absorbance of the clear supernatant was measured at 400 nm. In addition, image analysis of the intracellular GSH level was also assessed. After cells were incubated with 5 μM CMAC, a GSH sensitive fluorescence dye, for 30 min in the dark, cells were treated with AgNPs. The CMAC fluorescence images were analyzed by a Zeiss Axiovert 200 inverted microscope at an excitation wavelength of 351 nm and an emission wavelength of 380 nm (Tauskela et al., 2000).

2.8. Western blot analysis

Cells were lysed on ice for 30 min in 100 μl of lysis buffer (120 mM NaCl, 40 mM Tris pH

8.0, 0.1% NP 40) and centrifuged at 13,000×g for 15 min. The supernatants were collected from the lysates and the protein concentrations were determined. Aliquots of the lysates (40 μg of protein) were boiled for 5 min and electrophoresed in 10% SDS-polyacrylamide gel. The proteins in the gels were transferred onto nitrocellulose membranes (Bio-Rad, Hercules, CA, USA) and subsequently incubated with primary antibodies. The membranes were further incubated with secondary anti-immunoglobulin-G-horseradish peroxidase conjugates (Pierce, Rockford, IL, USA), followed by exposure to X-ray film. The protein bands were detected using an enhanced chemiluminescence western blotting detection kit (Amersham, Little Chalfont, Buckinghamshire, UK).

2.9. Single cell gel electrophoresis (Comet assay)

A comet assay was performed to determine the degree of oxidative DNA damage (Singh, 2000). Cells were exposed to AgNPs for 3 h, washed with PBS. The cell suspension was mixed with 75 μl of 0.5% low melting agarose (LMA) at 39 ℃, and spread on a fully frosted microscopic slide pre-coated with 200 μl of 1% normal melting agarose (NMA). After the solidification of the agarose, the slide was covered with another 75 μl of 0.5% LMA and then immersed in a lysis solution (2.5 M NaCl, 100 mM Na-EDTA, 10 mM Tris, 1% Trion X-100, and 10% DMSO, pH 10) for 1 h at 4 ℃. The slides were then placed in a gel-electrophoresis apparatus containing 300 mM NaOH and 10 mM Na-EDTA (pH 13) for 40 min to allow for DNA unwinding and the alkali labile damage. Next, an electrical field (300 mA, 25 V) was applied for 20 min at 4 ℃ to draw the negatively charged DNA toward an anode. After the electrophoresis, the slides were washed three times for 5 min at 4 ℃ in a neutralizing buffer (0.4 M Tris, pH 7.5), followed by staining with 75 μl of PI (20 μg/ml). The slides were observed using a fluorescence microscope and image analyzer (Kinetic Imaging, Komet 5.5, UK). The percentage of the total fluorescence in the tail and the length of the tail were

recorded in 50 cells per slide.

2.10. Lipid peroxidation assay

Lipid peroxidation was assayed by determination of 8-isoprostane levels (Manzer et al., 2006; Beauchamp et al., 2002). The levels of 8-isoprostane in the culture medium were determined using of a commercial enzyme immunoassay (Cayman Chemical, Ann Arbor, MI, USA) according to the manufacturer's instructions. Lipid peroxidation was also estimated using DPPP, a fluorescent probe (Okimotoa et al., 2000). After cells were incubated with 5 μM of DPPP for 15 min in the dark, cells were treated with AgNPs. The DPPP fluorescence images were analyzed using a Zeiss Axiovert 200 inverted microscope at an excitation wavelength of 351 nm and an emission wavelength of 380 nm.

2.11. Protein carbonyl formation

The amount of carbonyl formation in protein was determined using an Oxiselect^{TM} protein carbonyl ELISA kit purchased from Cell Biolabs (San Diego, CA, USA) according to the manufacturer's instructions.

2.12. Nuclear staining with Hoechst 33342

Hoechst 33342, which is a DNA-specific fluorescent dye, was added to each well and incubated for 10 min at 37 ℃. The stained cells were visualized under a fluorescent microscope, equipped with a CoolSNAP-Pro color digital camera to examine the degree of nuclear condensation.

2.13. Detection of apoptotic sub-G_1 hypodiploid cells

The percentage of apoptotic sub-G_1 hypodiploid cells was determined using flow cytometer

(Nicoletti et al., 1991). Cells were fixed in 1ml of 70% ethanol for 30 min at 4 ℃, then washed twice with PBS, and incubated for 30 min in the dark at 37 ℃ in 1 ml of PBS containing 100 μg of propidium iodide and 100 μg of RNase A. A flow cytometric analysis was performed using a FACSCalibur flow cytometery. The percentage of sub-G_1 hypodiploid cells was assessed based on the histograms generated by the Cell Quest and Mod-Fit computer programs.

2.14. DNA fragmentation

The level of cellular DNA fragmentation was assessed by analyzing cytoplasmic histone-associated DNA fragmentation using a kit from Roche Diagnostics (Portland, OR, USA) according to the manufacturer's instructions.

2.15. $\Delta\psi_m$ analysis

Mitochondrial $\Delta\psi$ was analyzed using JC-1, a lipophilic cationic fluorescence dye. JC-1 was added to each well and incubated for an additional 30 min at 37 ℃. After washing with PBS, the stained cells were assayed using a flow cytometer. For image analysis of mitochondrial $\Delta\psi$, the stained cells were mounted onto microscope slide in mounting medium.Microscopic images were collected using the Laser Scanning Microscope 5 PASCAL program on a confocal microscope (Cossarizza et al., 1993).

2.16. Transient transfection of siRNA

Cells were seeded at 1.5×10^5 cells/well in a 24-well plate and allowed to reach approximately 50% confluence on the day of transfection. The siRNA constructs used were amismatched siRNA control and siRNA against JNK. Cells were transfected with 10-50 nM siRNA using lipofectamine[TM] 2000 (Invitrogen, Carlsbad, CA) based on the manufacturer's instruction. At 24 h after transfection, the cells were treated with AgNPs for 48 h and examined

by either Western blot or MTT assay.

2.17. Statistical analysis

All measurements were made in triplicate and all values were expressed as the means±standard error of the mean (SEM). The results were subjected to an analysis of variance (ANOVA) using the Tukey test to analyze the difference. Values of $p < 0.05$ were considered significant.

3. RESULTS

3.1. AgNPs induce cytotoxicity

AgNPs and AgNO$_3$ showed cytotoxicity in a dose-dependent manner in human Chang liver cells (Fig. 1A). AgNPs showed higher cytotoxicity compared to AgNO$_3$ because the IC$_{50}$ (concentration yielding 50% growth inhibition) of AgNPs and AgNO$_3$ were about 4 and 8 μg/ml, respectively. The concentration of AgNPs corresponding to the IC$_{50}$ (4 μg/ml) was used as optimal concentration for further study. To determine AgNPs incorporation into cells, phase contrast inverted microscopy was utilized. As shown in Fig. 1B, AgNPs-treated cells were observed to have increased intracellular AgNPs concentrations compared to untreated cells (control).

A
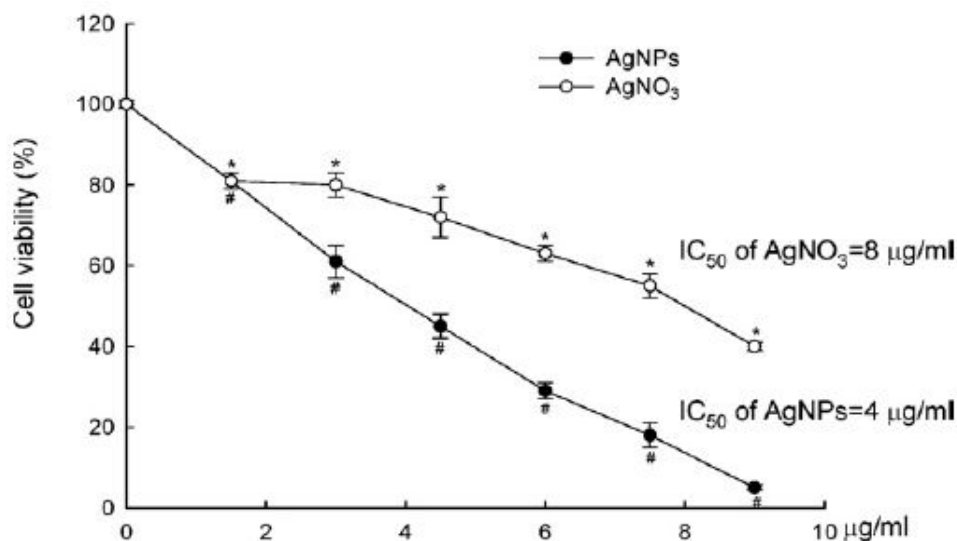
Fig. 1. Cytotoxicity induced by AgNPs in human Chang liver cells. (A) Cells were treated with AgNPs and AgNO$_3$ at various concentrations for 24 h, and cytotoxicity was determined by the MTT method. Calculated IC$_{50}$ values are shown in the upper right corner of each curve. Data represent mean±SEM. * and # denote significant differences from untreated cells of AgNPs and AgNO$_3$, respectively ($p < 0.05$).

B
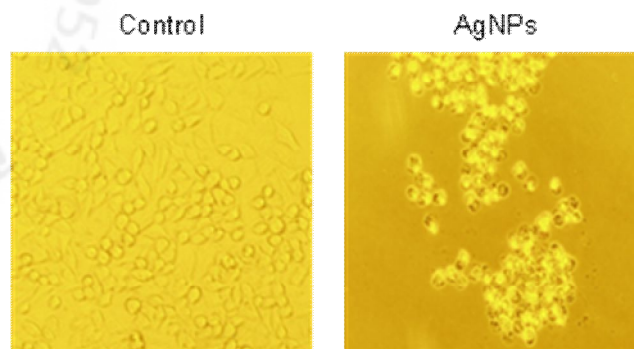
Fig. 1. continued. (B) Incorporation of AgNPs into cells was visualized by inverted microscopy (magnification 100×).

3.2. AgNPs induce ROS

Oxidative stress has been cited as one of the more important mechanisms of toxicity related to nanoparticle exposure (Nel et al., 2006). To investigate the potential role of oxidative stress induced by AgNPs, ROS generation was measured. As shown in Fig. 2A, the ROS levels generated in response to AgNPs were significantly maintained for 12 h, and AgNPs-induced ROS were suppressed by NAC, a synthetic antioxidant. This pattern was also confirmed byflowcytometric data that showing a fluorescence intensity of 341 in AgNPs-treated cells at 3 h compared to 146 in control cells (Fig. 2B). Confocal microscopy illustrated that the red fluorescence intensity of ROS was enhanced in AgNPs-treated cells compared to control cells (Fig. 2C). These results suggest that AgNPs results in the production of ROS.

A
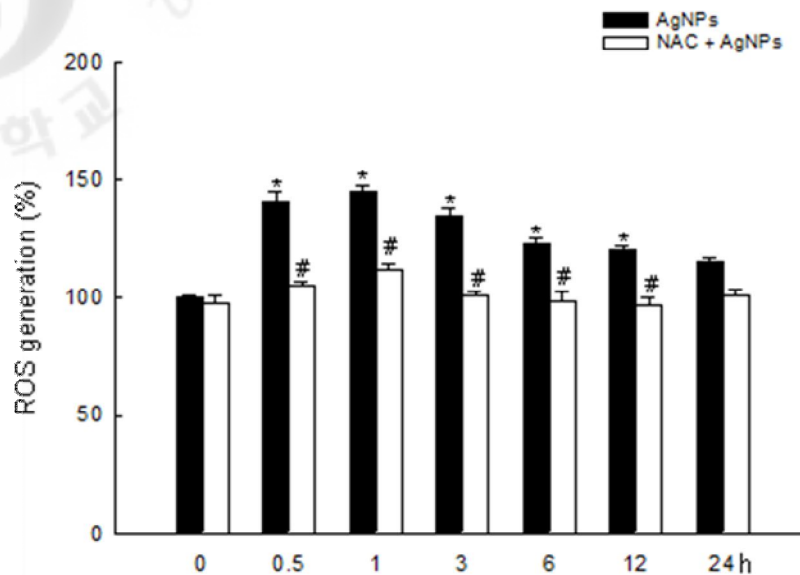
B
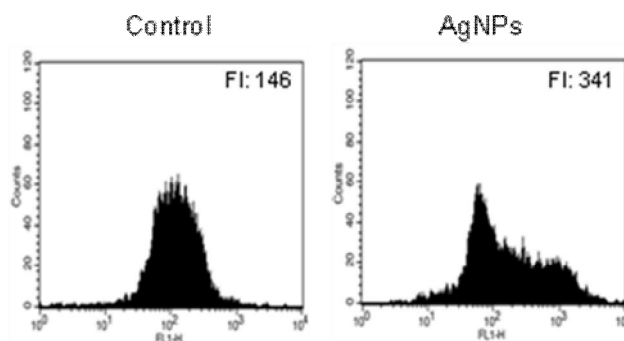
Fig. 2. Generation of intracellular ROS in response to AgNPs. Generation of intracellular ROS was detected by spectrofluorometry (A) and flow cytometry (B) after DCF-DA treatment. The values were expressed as means±SEM. *Significantly different from control ($p < 0.05$), and #significantly different from AgNPs-treated cells ($p < 0.05$). FI: fluorescence intensity of DCF-DA.

C
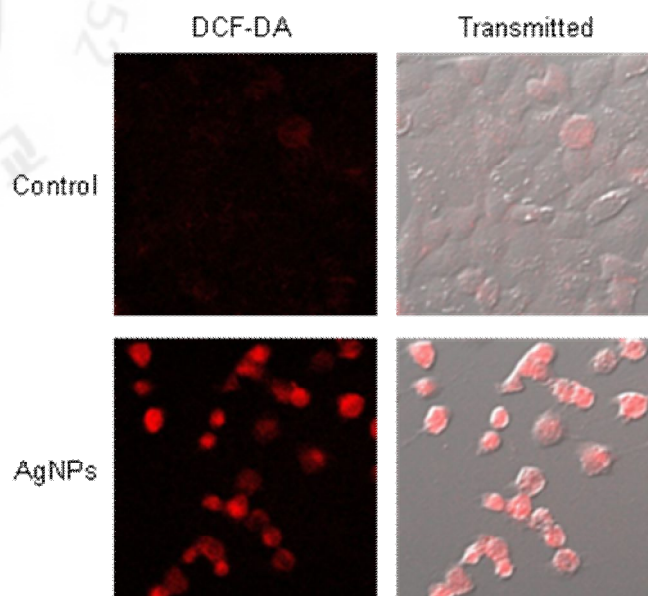
Fig.2. continued. (C) The representative confocal images illustrate the increase in red fluorescence intensity of DCF produced by ROS in AgNPs-treated cells compared to the control (original magnification 400×).

3.3. The effect of AgNPs on reduced glutathione

GSH is a sulfhydryl-containing molecule present in cells that is responsible for maintaining cellular oxidation–reduction homeostasis. Alterations in GSH level can be monitored as an indication of oxidative stress in cells. GSH is formed by γ-glutamate cystein ligase (γ-GCL) and GSS. The protein expression of the catalytically active subunit of γ-GCL (GCLC) and GSS was decreased by AgNPs treatment in time dependent manner (from 0.5 h to 24 h) (Fig. 3A). Similarly, AgNPs treatment decreased GSH levels as measured in colorimetric assay system in a timedependent manner, and NAC pretreatment in AgNPs-treated cells restored it via scavenging of ROS (Fig. 3B). The confocal microscopic data illustrated that the blue fluorescence intensity of cellular GSH was decreased in AgNPs-treated cells compared to

−16−

control cells (Fig. 3C). HR-MAS NMR can be used with bio-fluids, tissues and cells for the identification and quantification of metabolites (Bayet-Robert et al., 2010). GSH signals appear at δ 2.2 ppm (quartet), 2.5 ppm (multiplet), 2.9 ppm (multiplet) and 3.8 ppm (multiplet). The NMR spectra in our study detect GSH in the 2.51–2.55 ppm range and AgNPs treatment nearly depleted GSH levels (Fig. 3D). These results suggest that GSH levels depleted by AgNPs were due to decrease levels of GCLC and GSS and ultimately resulted in oxidative stress.

Fig. 3. Effects of AgNPs on cellular glutathione systems. (A) Cell lysates were electrophoresed and GCLC and GSS proteins were detected using specific antibodies. Levels of GSH were detected using (B) a GSH content assay kit. The values were expressed as means±SEM. *Significantly different from control ($p < 0.05$), and #significantly different from AgNPs-treated cells ($p < 0.05$).
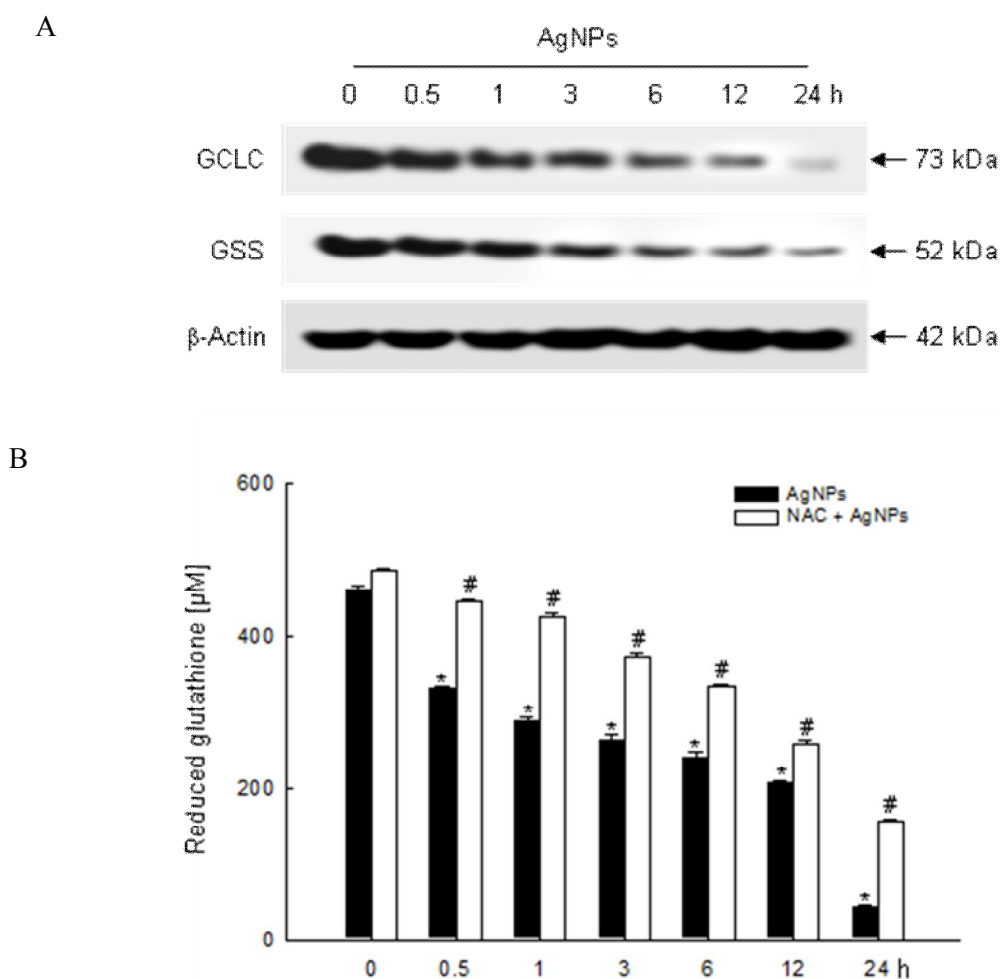
C
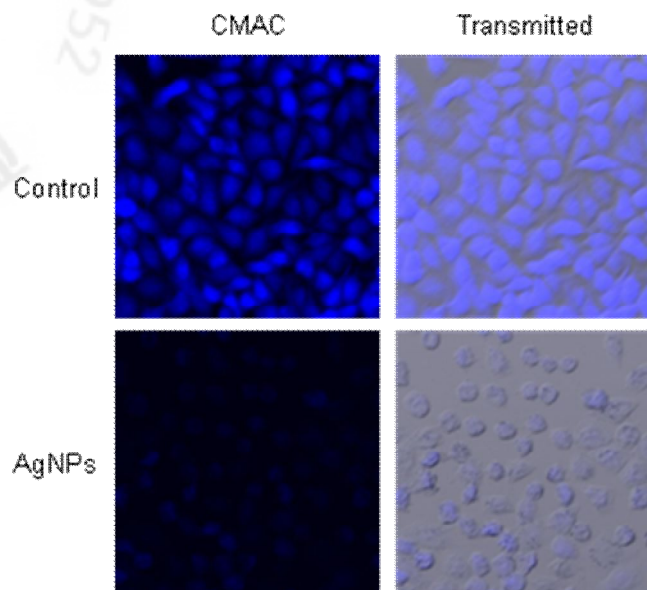
D
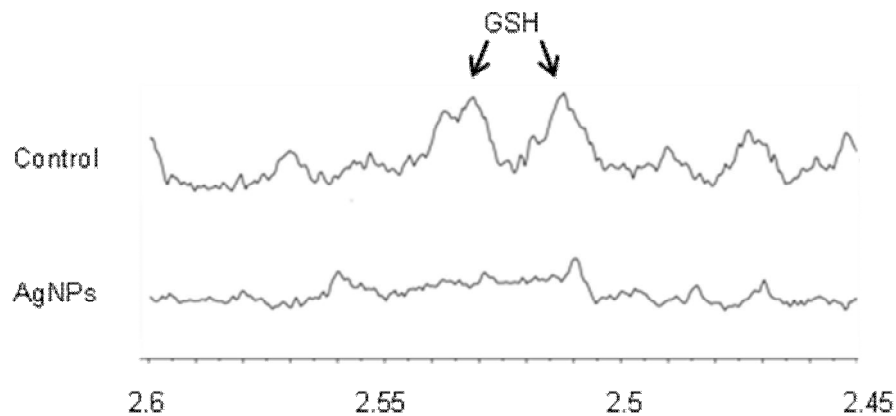
Fig. 3. continued. Levels of GSH were detected using (C) confocal microscopy after fluorescent probe CMAC staining, and (D) HR-MAS NMR spectroscopy.

3.4. Oxidative stress induced by AgNPs damages cellular components

AgNPs treatment increased the tail length and percentage of DNA in the tails compared to control cells (Fig. 4A). AgNPs-treated cells showed increases in lipid peroxidation as measured by the levels of 8-isoprostane and by microscopic observation after staining with DPPP, a

-18-

specific fluorescence probe that detects lipid peroxidation in the cell membrane (Figs. 4B and C). Protein carbonyl formation serves as a biomarker for cellular oxidative damage (Stadtman, 1993). The protein carbonyl content was increased in AgNPs-treated cells compared to control cells (Fig. 4D). These results suggest that AgNPs damages cellular components via oxidative stress.

A
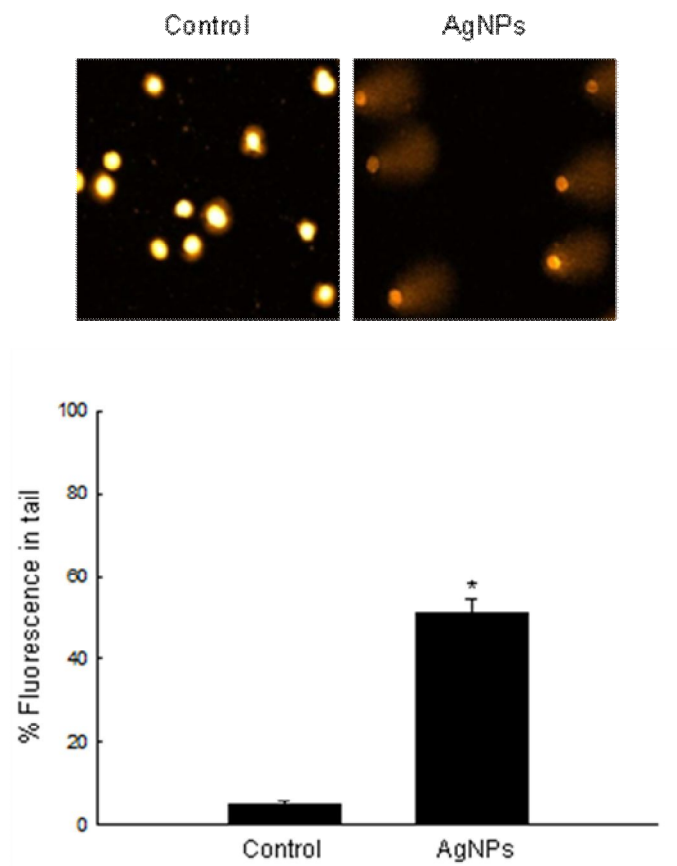
Fig. 4. Oxidative stress-induced damage to cellular components by AgNPs. (A) Representative images and percentage of cellular DNA damage were detected using an alkaline comet assay. The values are expressed as means±SEM. *Significantly different from control cells ($p < 0.05$).

B
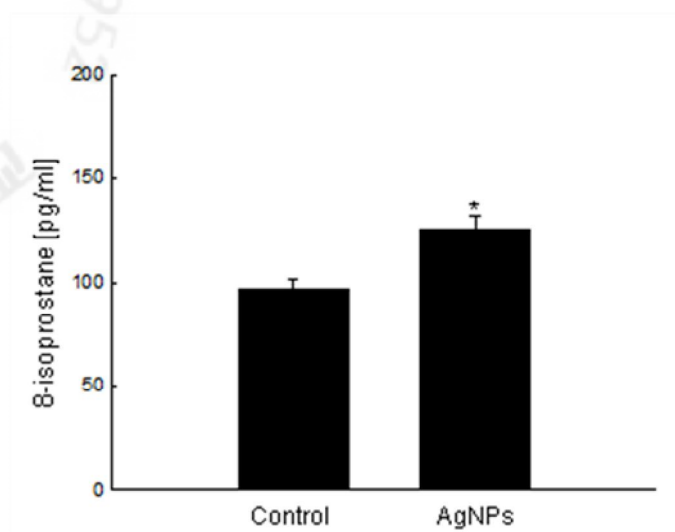
C
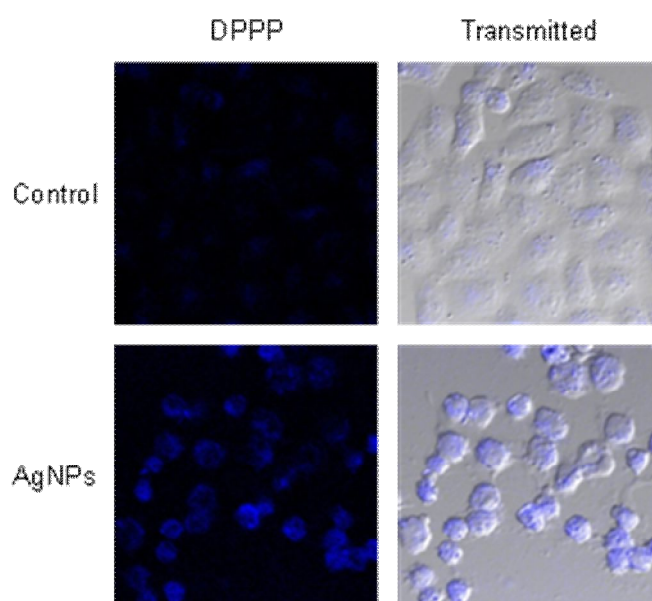
Fig. 4. continued. Lipid peroxidation was assayed by (B) measuring the level of 8-isoprostane and (C) detected using confocal microscopy after DPPP fluorescence staining. The values are expressed as means±SEM. *Significantly different from control cells ($p < 0.05$).

D
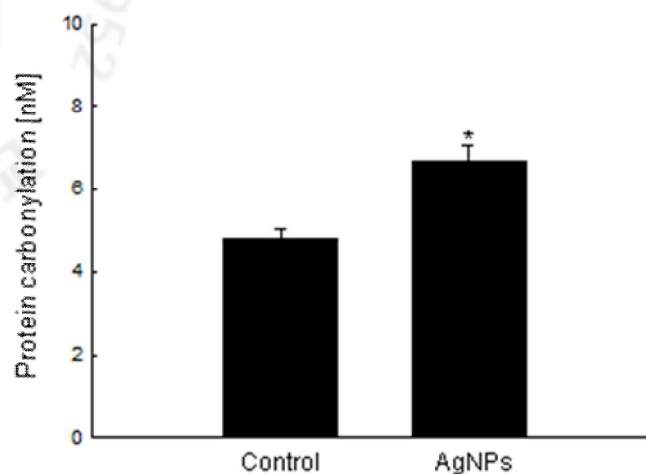
Fig. 4. continued. (D) Protein oxidation was assayed by measuring the amount of carbonyl formation. The values are expressed as means±SEM. *Significantly different from control cells ($p < 0.05$).

3.5. AgNPs induce apoptosis via a mitochondria- and caspase-dependent pathway

To evaluate the cytotoxic effects of AgNPs in terms of apoptosis, the cellular nuclei were stained with Hoechst 33342 and assessed by microscopy. The microscopic pictures in Fig. 5A revealed that the control cells had intact nuclei, while the AgNPs-treated cells showed significant nuclear fragmentation, which is indicative of apoptosis. However, NAC pretreatment in AgNPs-treated cells showed a decrease in nuclear fragmentation. An analysis of the apoptotic sub-G_1 DNA content in the AgNPs-treated cells revealed a 28% increase compared to control cells (Fig. 5B). In addition, AgNPs treatment increased the levels of cytoplasmic histone-associated DNA fragmentation (Fig. 5C). During the apoptotic process, the mitochondrial membrane pores are opened and $\Delta\psi_m$ was disrupted (Zamzami et al., 1996). As shown in Fig. 5D, JC-1 staining data showed that AgNPs-treated cells exhibited a decrease in red fluorescence (polarized state) and an increase in green fluorescence (depolarized state). Bcl-2 prevents the opening of the mitochondrial membrane pore and Bax accelerates it (Zamzami et al., 1995).

Pore opening results in the loss of $\Delta\psi_m$, which induces the release of cytochrome c from mitochondria (Zhivotovsky et al., 1998). As shown in Fig. 5E, AgNPs treatment resulted in a decrease in Bcl-2 expression and an increase in Bax expression in a time dependent manner; the Bax/Bcl-2 ratio was 1.0, 7.0, 9.5, 12.8 and 24.5 at 0 h, 6 h, 12 h, 24 h, and 48 h after AgNPs tratment, respectively. The change in the Bax/Bcl-2 ration led to the release cytochrome c from the mitochondria into the cytosol. AgNPs led to the active forms of caspase 9 and caspase 3 (a target of caspase 9) in time-dependent manner (from 6 h to 48 h), which are activated in response to mitochondrial membrane disruption. These results suggest that AgNPs-induced apoptosis signals through a caspase-dependent pathway with mitochondrial involvement.

A
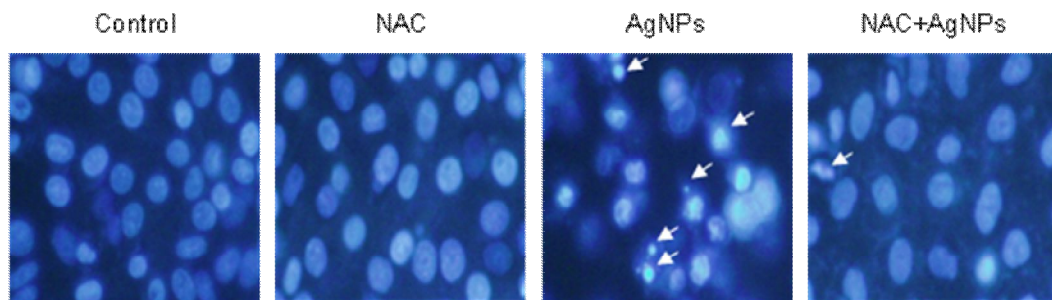
B
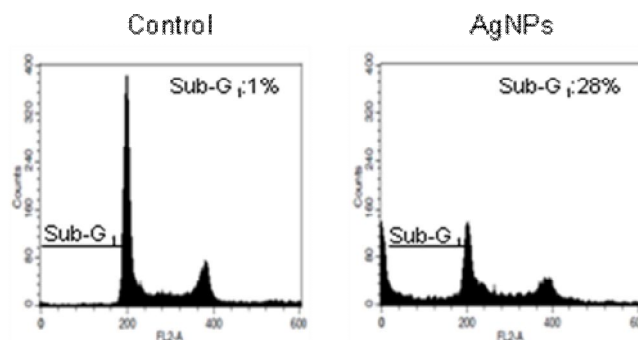
Fig. 5. Apoptosis induced by AgNPs. (A) Apoptotic body formation was observed under a fluorescent microscope after Hoechst 33342 staining. The apoptotic bodies are indicated with arrows. (B) The apoptotic sub-G_1 DNA content was detected using flow cytometer after propidium iodide staining.

C

D

Mitochondrial ΔΨ

Polarized state   Depolarized state

Control

AgNPs
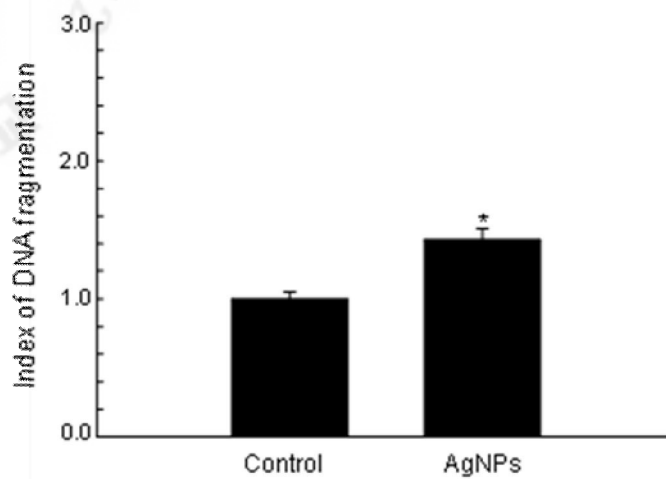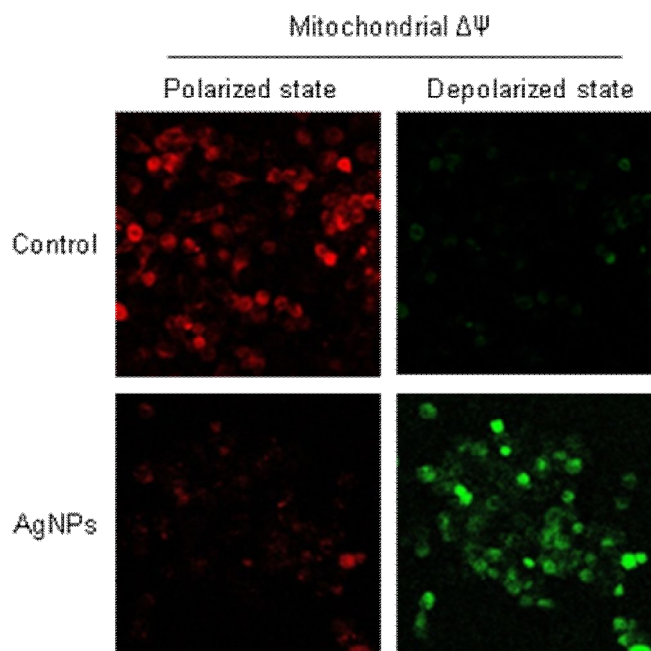
Fig. 5. continued. (C) DNA fragmentation was quantified using an ELISA kit. The values are expressed as means±SEM. *Significantly different from control cells ($p < 0.05$). (D) The $\Delta\psi_m$ was analyzed with confocal microscopy after staining of cells with JC-1.

E
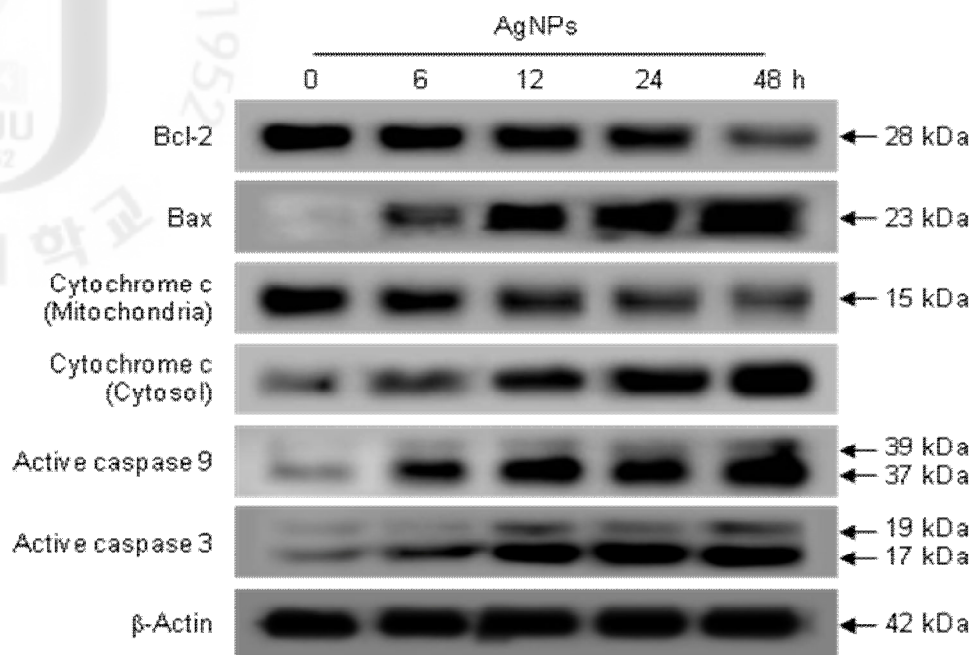
Fig. 5. continued. (E) Bcl-2, Bax, mitochondria and cytosol cytochrome c, caspase 9, and caspase 3 were detected using specific antibodies.

3.6. AgNPs-induced apoptosis requires JNK activation

AgNPs induced JNK phosphorylation (the active form of JNK) in a time-dependent manner (from 1 h to 24 h) (Fig. 6A). Pretreatment with SP600125 attenuated AgNPs-induced cytotoxicity (Fig. 6B). Likewise, transfection with siRNA against JNK abolished AgNPs-induced death (Fig. 6C), suggesting that JNK is involved in AgNPs-mediated apoptosis.

A
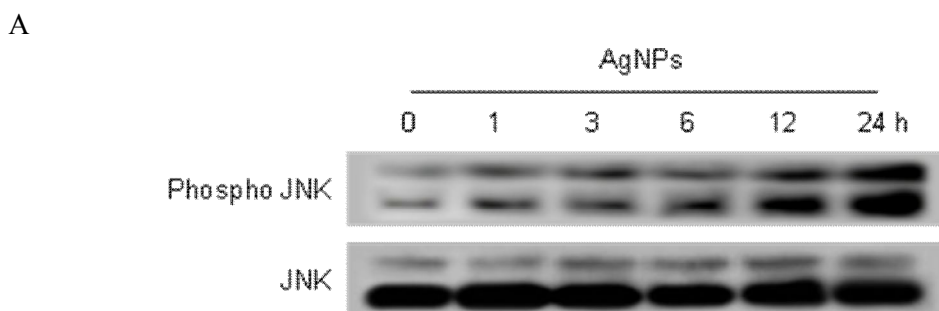
Fig. 6. Activation of JNK by AgNPs. (A) Phospho JNK and JNK were detected using specific antibodies.

B
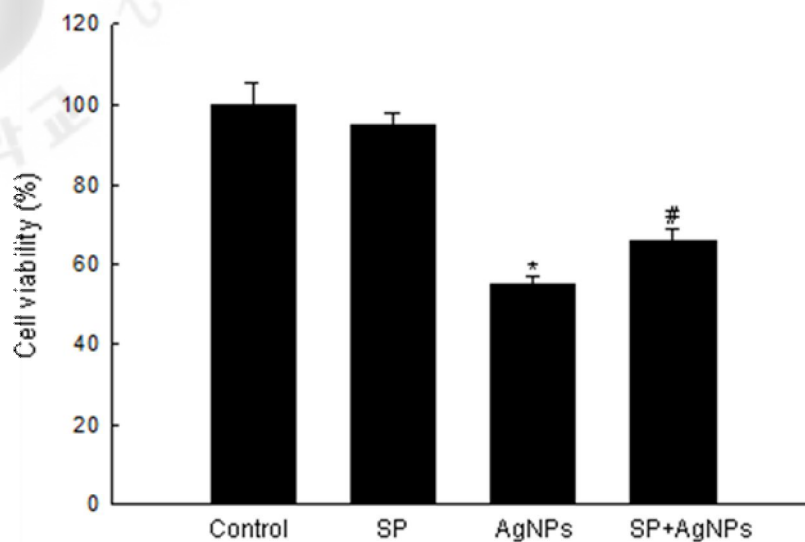
C
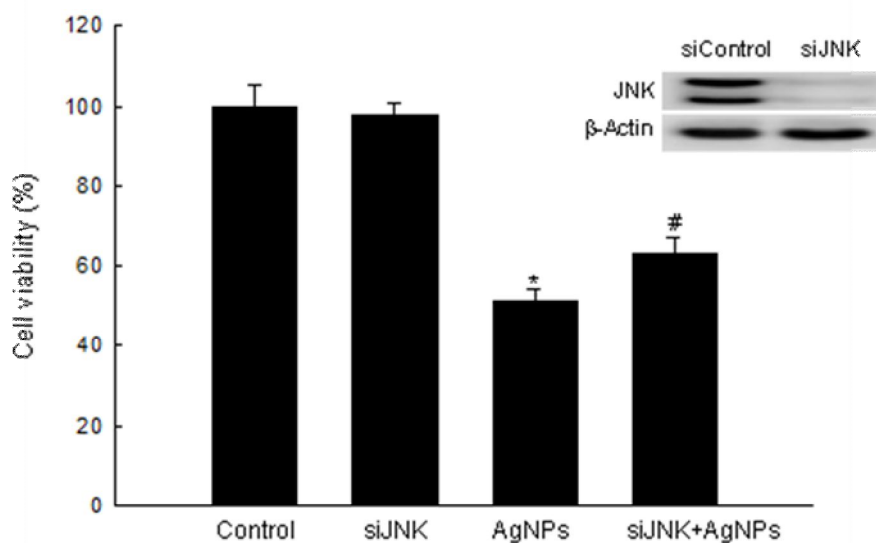
Fig. 6. continued. (B) Cells were pre-incubated with SP600125 for 1 h, followed by incubation with AgNPs for 24 h. Cell viability was measured using the MTT assay. (C) Cells were transfected with siControl and siJNK RNA. At 24 h after transfection, the cells were treated with AgNPs for 24 h and cell viability was measured using the MTT assay. *Significantly different from control ($p < 0.05$), and #significantly different from AgNPs-treated cells ($p < 0.05$).

4. Discussion

Our studies provided evidence for a molecular mechanism via which AgNPs induce cell damage via the generation of ROS and the induction of apoptosis. In our system, using phase contrast inverted microscopy, AgNPs-treated cells were observed to have increased intracellular AgNPs concentrations compared to cells without AgNPs treatment. Díaz et al. (2008) studied the uptake of 5 types of nanoparticles by human blood cells and tumor cell lines and observed the appearance of groups of nanoparticles inside the human monocyte as the nanoparticles were rapidly taken up by the cells. Uptake of AgNPs via micelles has been reported (Luoma, 2008); however, the pathway by which AgNPs enter cells has not been clearly identified. Therefore, more comprehensive observation of the cellular uptake of AgNPs will be addressed in future studies.

Consistent with previous reports that nano-materials provoke oxidative stress (Harhaji et al., 2007; Limbach et al., 2007; Lin and Beal, 2006), our results showed that AgNPs induced ROS generation. Moreover, ROS generation in AgNPs-treated cells was decreased by pre-treatment of cells with NAC. GSH acts directly as a scavenger of ROS and as a substrate for GSH peroxidase to reduce hydrogen peroxide (Habib et al., 2007; Peña-Llopis et al., 2003; Vairetti et al., 2001). GSH is the major endogenous antioxidant scavenger that protects cells from oxidative stress through its ability to bind to and reduce ROS. Thus, preserving the GSH-mediated antioxidant defense is critical for cell survival (Anderson et al., 2004; Dewanjee et al., 2009; Sies, 1999). GSH is formed by γ-GCL and GSS. γ-GCL catalyzes the first and rate-limiting step in the process that yields glutamylcysteine in cellular GSH biosynthesis. The final step is catalyzed by GSS and adds a glycine residue to form glutamylcysteinylglycine or glutathione. γ-GCL is a heterodimeric enzyme composed of a catalytically active subunit (GCLC) that possesses all of the substrate-binding sites and a modifier subunit (GCLM) that

regulates GCLC's affinity for substrates and inhibitors (Cortes-Wanstreet et al., 2009). Our results showed that AgNPs decreased GSH levels through the inhibition of GSH synthesizing enzymes (GCLC and GSS), leading to the generation of ROS. However, GSH is not the only intracellular antioxidant defense. Therefore, it remains to be determined if the other intracellular antioxidant systems (e.g. superoxide dismutase, catalase) are also impaired by AgNPs.

Highly reactive hydroxyl radicals attack cellular components including DNA, lipids, and proteins to cause various kinds of oxidative damages (Denisova et al., 2001; Halliwell and Aruoma, 1991). AgNPs were found to increase the DNA tail length in a comet assay, which measures DNA strand breaks as well as alkali labile sites (Rajagopalan et al., 2003; Singh, 2000). Cell membrane lipids peroxidation by AgNPs was shown using the DPPP and 8-isoprostane assays. In addition, oxidative damage to amino acid residues in proteins results in the formation of carbonyl derivatives and can compromise cellular integrity (Hawkins and Davies, 2001). The protein carbonyl content in cells increased significantly in AgNPs-treated cells.DNAdamage, lipid peroxidation, and protein oxidation result from AgNPs-induced intracellular GSH depletion and ROS generation, leading to damage to cellular components.

Recently several studies have shown that AgNPs trigger apoptosis via ROS generation in in vitro systems (Ahamed et al., 2010a; Foldbjerg et al., 2009). However, the function of ROS in AgNPsinduced liver cells death is currently unclear. The time-dependent decrease in ROS shown in Fig. 2A is probably due to cell death. To explore the possible molecular mechanisms of AgNPs-mediated cell death, we measured changes in the levels of regulators involved in apoptosis. Mitochondria are important signaling centers during apoptosis, and the loss of mitochondrial integrity can be induced or inhibited by many regulators of apoptosis (Green and Reed, 1998; Kroemer et al., 1997). In many cases, oxidative stress induces caspase activation through cytochrome c release from the mitochondrial inter-membrane space into the cytosol (Green and Reed, 1998; Liu et al., 1996). In our study, AgNPs induced mitochondrial release of

cytochrome c and the loss of $\Delta\psi_m$. During the apoptotic process, Bcl-2 prevents the opening of the mitochondrial membrane pores, whereas Bax induces the opening of membrane pores (Zamzami et al., 1995).Weshowed in this study that loss of $\Delta\psi_m$ by AgNPs is a result of down-regulation of Bcl-2, and up-regulation of Bax. Cytochrome c release initiates a cascade that leads to the activation of caspase 3 through Apaf-1 and caspase 9 (Li et al., 1997; Zou et al., 1997). Our results also demonstrated that cytochrome c was released from mitochondria into the cytoplasm, followed by caspase 9 and caspase 3 activation. Hsin et al. (2008) have reported that mitochondria are a major site for AgNPs-induced ROS generation. This suggests that AgNPs activates the intrinsic apoptotic pathway, which is characterized by modulation of Bax and Bcl-2 expressions, disruption of $\Delta\psi_m$, and cytochrome c release from the mitochondria. The apoptotic process is regulated by many intracellular signaling pathways, including the JNK pathway (Chang and Karin, 2001; Davis, 2000; Lin, 2003; Shaulian and Karin, 2002). Other studies have reported that JNK is involved in various oxidative stress-associated diseases (Czaja, 2003; Shen and Liu, 2006) and that ROS generation could result in sustained JNK activation (Kamata et al., 2005). Among the pro-apoptotic targets of JNK Bcl-2 regulates apoptotic initiation via the prevention of cytochrome c release from the mitochondria (Yang et al., 1997). JNK participates in apoptotic signaling via phosphorylation of Bcl-2, which results in Bcl-2 inactivation (Herr and Debatin, 2001; Srivastava et al., 1999).

In conclusion, AgNPs induced ROS generation and intracellular GSH depletion and led to damage to cellular components. Additionally, AgNPs led to apoptosis via mitochondria-dependent and caspase-dependent pathways mediated by JNK (Fig. 7).
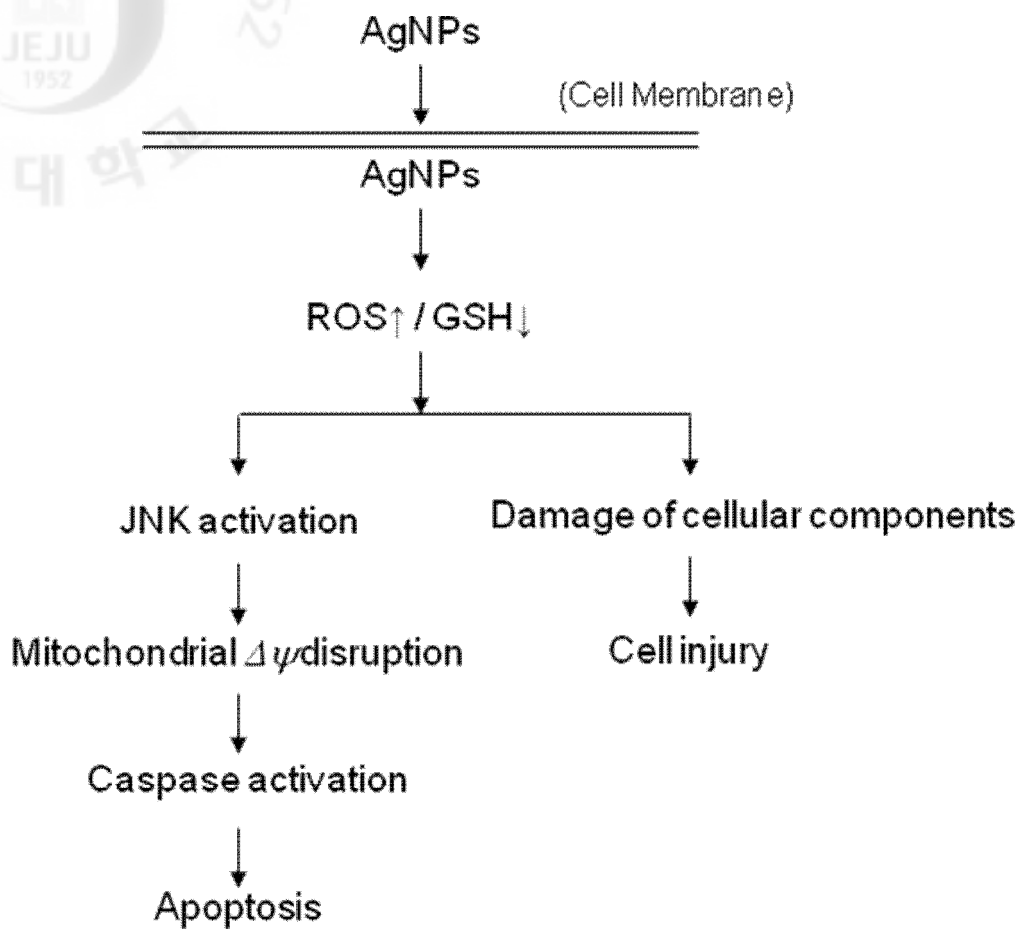
Fig. 7. A proposed pathway for AgNPs-induced ROS generation and intracellular GSH depletion, damage to cellular components, and apoptosis.

PART II

Silver nanoparticles down-regulate Nrf2-mediated 8-oxoguanine

DNA glycosylase 1 through inactivation of extracellular

regulated kinase and protein kinase B in human Chang liver cells

ABSTRACT

Recently, we reported that AgNPs induced ROS generation and the resultant oxidative stress contributes to the cell damage associated with AgNPs. 8-oxoG is sensitive marker of ROS-induced DNA damage. OGG1 is an important DNA repair enzyme that recognizes and excises 8-oxoG. The aim of the present study was to examine the effect of AgNPs-induced oxidative stress on OGG1 and to elucidate mechanisms underlying AgNPs toxicity. AgNPs decreased OGG1 mRNA and protein expression, resulting in decreased OGG1 activity. Decreased OGG1 activity in AgNPs-treated cells led to increased 8-oxoG levels. The transcription factor Nrf2 is an important factor in the inducible regulation of OGG1. AgNPs treatment decreased nuclear Nrf2 expression, translocation into nucleus, and transcriptional activity of Nrf2. ERK and AKT, which are upstream of Nrf2, contribute to OGG1 expression. AgNPs attenuated both active forms of ERK and AKT protein expression, resulting in suppression of Nrf2 and decrease of OGG1 expression. These studies demonstrate that down-regulation of Nrf2-mediated OGG1 in exposure to AgNPs occurs through ERK and AKT inactivation.

Keywords: Silver nanoparticles; 8-Oxoguanine DNA glycosylase 1; 8-Oxoguanine; NF-E2-related factor 2.

1. INTRODUCTION

AgNPs are an important class of nanomaterials for a wide range of industrial and medical applications. Despite their widespread use, AgNPs are toxic to a variety of organs, including the lung, liver, and brain (Ahamed et al., 2010b). Possible mechanisms of AgNPs toxicity include induction of ROS, oxidative stress, DNA damage and apoptosis (Ahamed et al., 2010b). It has been demonstrated, for example, that AgNPs enter fibroblasts and hepatocytes and cause DNA damage and apoptosis (Arora et al., 2009). We recently reported that AgNPs cause cytotoxicity by oxidative stress-induced apoptosis and damage to DNA, lipid and protein (Piao et al., 2011).

8-oxoG is one of the most commonly formed DNA lesions and is considered a cellular marker for both oxidative stress and DNA damage (Dizdaroglu et al., 2002). OGG1 is the first step and rate-limiting enzyme involved in the removal of 8-oxoG through the base excision repair (BER) pathway (Boiteux and Radicella, 2000; Klungland et al., 1999; de Souza-Pinto et al., 2001). The human OGG1 promoter contains a putative transcription factor Nrf2 binding site and Nrf2 leads to OGG1 transcription (Merrill et al., 2002; Dhénaut et al., 2000). Mitogen activated protein kinase (MAPK) and AKT are important signaling enzymes involved in the transduction of various signals from the cell surface to the nucleus. MAPK and AKT induce Nrf2 translocation or increased stability, which leads to increased Nrf2 activity (Zipper and Mulcahy, 2003; Wang et al., 2008).

In this study, we investigated whether AgNPs-mediated ROS induction can affect DNA base modification with respect to 8-oxoG and studied the mechanisms by which the 8-oxoG is achieved.

2. MATERIALS AND METHODS

2.1. Reagents

AgNPs were provided by professor Jinhee Choi of Seoul University (Seoul, Repubilc of Korea) and characterization of AgNPs was conducted as described previously (Eom and Choi, 2010). AgNPs had an even distribution, with individual particle sizes ranging from 5 to 10 nm. AgNPs tend to agglomerate when exposed to cells; the most of the AgNPs in the medium were of about 28-35 nm in size. Ag ions were estimated using a multitype inductively coupled plasma emission spectrometer (ICPE-9000, Shimadzu, Tokyo, Japan). The concentrations of AgNPs and Ag ions had equivalent Ag masses and measured prior to exposure of the compounds to cell culture media. The OGG1 promoter-luciferase construct was a generous gift from Professor Ho Jin You of Chosun University (Gwangju, Republic of Korea). OGG1 antibody was purchased from Abcam (Cambridge, MA, USA). ERK2, phospho ERK1/2, Nrf2, and β-actin antibodies were purchased from Santa Cruz Biotechnology (Santa Cruz, CA, USA). Phospho AKT (Ser 473) and AKT antibodies were purchased from Cell Signaling Technology (Beverly, MA, USA). Avidin-tetramethylrhodamine isothiocyanate (TRITC) conjugate was purchased from Sigma Chemical Company (St. Louis, MO, USA). Other chemicals and reagents were of analytical grade.

2.2. Cell culture

Human Chang liver cells were obtained from the American type culture collection (Rockville, MD, USA) and were maintained in an incubator with a humidified atmosphere of 5% CO_2 at 37 ℃. Cells were cultured in RPMI-1640 medium containing 10% heat-inactivated fetal calf serum, streptomycin (100 μg/ml) and penicillin (100 U/ml).

2.3. Transient transfection and OGG1 promoter luciferase assay

Cells were transiently transfected with a plasmid harboring the OGG1 promoter using the transfection reagent DOTAP according to the manufacturer's instructions (Roche, Mannheim, Germany). After overnight transfection, cells were treated with AgNPs for 6-48 h. Cells were then lysed with reporter lysis buffer (Promega, Madison, WI, USA), and the lysate supernatant was mixed with the luciferase assay reagent. The mixture was placed in a luminometer to measure the light produced.

2.4. Reverse transcription-polymerase chain reaction (RT-PCR)

Total RNA was isolated from cells using Trizol (GibcoBRL, Grand Island, NY, USA). PCR conditions for OGG1 and for the housekeeping gene GAPDH were: 35 cycles of 94 ℃ for 2 min; 94 ℃ for 20 s; 58 ℃ for 30 s; 72 ℃ for 1 min; and 72 ℃ for 5 min. The primer pairs (Bionics, Seoul, Republic of Korea) were as follows (sense and antisense, respectively): human OGG1-sense 5'-CTGCCTTCTGGACAATCTTT-3' and human OGG1-antisense 5'-TAGCCCGCCCTGTTCTTC-3', and human GAPDH sense 5'-GCAGTGAGGGTCTCTCTCCT-3'; and human GAPDH antisense 5'-AAGGTCGGAGTCAACGGATT-3'. Amplified products were resolved by 1% agarose gel electrophoresis, stained with ethidium bromide, and photographed under ultraviolet light.

2.5. Western blot analysis

Cells were lysed on ice for 30 min in 100 μl of lysis buffer [120 mM NaCl, 40 mM Tris (pH 8), 0.1% NP 40] and centrifuged at 13,000 × g for 15 min. The supernatants were collected from the lysates and the protein concentrations were determined. Aliquots of the lysates (40 μg of protein) were boiled for 5 min and electrophoresed in a 10% SDS–polyacrylamide gel. The blots in the gels were transferred onto nitrocellulose membranes, and subsequently incubated

with primary antibodies. The membranes were further incubated with secondary anti-immunoglobulin-G-horseradish peroxidase conjugates (Pierce, Rockford, IL, USA), followed by exposure to X-ray film. The protein bands were detected using an enhanced chemiluminescence Western blotting detection kit (Amersham, Little Chalfont, Buckinghamshire, UK).

2.6. Transfection of cells with 8-oxoG-containing molecular beacon

Cells were seeded at 1×10^5 cells/well in 24-well plates and treated with 4 μg/ml of AgNPs for 24 h. An 8-oxoG-containing oligonucleotide with the sequence 5'- FAM-GCACTOAAGCGCCGCACGCCATGTCGACGCGCTTCAGTGC-DAB-3' (where O is 8-oxoG) was synthesized by Bioneer Corporation (Bioneer, Republic of Korea). The 5'-fluorophore (fluorescein amidite, FAM) is in close proximity to the 3'-quencher (4-(4'-dimethylaminophenylazo) benzoic acid, DAB). After being cut the beacon by OGG1, the fluorescent signal is liberated, forming the bases of detection of OGG1 activity. The beacon was dissolved in sodium chloride-tris-EDTA buffer to give a stock solution (100 pmol/μl). The beacon was heated for 5 min at 95 ℃, vortexed and then left to cool slowly to room temperature in the dark to permit the adoption of the correct stem-loop conformation of oligonucleotide. Prior to use, the beacon was diluted to 10 pmol/μl in distilled deionized water and 100 pmol beacon and 2 μl Lipofectamine™ 2000 (Invitrogen, Carlsbad, CA, USA) were transfected to cells. Cells were then placed in a humidified chamber (37 ℃, 5% CO_2) for 6 h. The green foci and fluorescence intensity were examined by both confocal microscopy and flow cytometry, respectively.

2.7. Detection of 8-oxoG

Cells were seeded in a plate at a concentration of 1×10^5 cells/ml and treated with AgNPs at

16 h after plating. After incubation for an additional 24 h at 37 ℃, cellular DNA was isolated using DNAzol reagent (Life Technologies, Grand Island, NY, USA) and quantified using a spectrophotometer. The amount of 8-hydroxy-2'- deoxyguanosine (8-OHdG, a nucleoside of 8-oxoG) in DNA was determined using 8-OHdG-EIA^{TM} kit from OXIS Health Products (Portland, OR, USA) according to the manufacturer's instructions. The amount of 8-oxoG was also estimated in a fluorescent binding assay (Struthers et al., 1998). Cells were fixed and permeabilized with ice-cold methanol for 15 min. 8-OxoG was visualized with avidin-conjugated TRITC under a fluorescence microscope.

2.8. Immunocytochemistry

Cells plated on coverslips were fixed with 4% paraformaldehyde for 30 min and permeabilized with 0.1% Triton X-100 in PBS for 2.5 min. Cells were then treated with blocking solution (3% bovine serum albumin in PBS) for 1 h and incubated with Nrf2 antibody diluted in blocking solution for 2 h. Immuno reacted primary Nrf2 antibody was detected by a 1:500 dilution of FITC-conjugated secondary antibody (Jackson Immuno Research Laboratories, West Grove, PA, USA) for 1 h. After washing with PBS, stained cells were mounted onto microscope slides in mounting medium with DAPI (Vector, Burlingame, CA, USA). Images were collected using the LSM 510 program on a Zeiss confocal microscope.

2.9. Chromatin immunoprecipitation (ChIP) assay

Cells were processed using the Simple ChIP^{TM} enzymatic chromatin IP kit from Cell Signaling Technology according to the manufacturer's instructions. Briefly, the procedure was initiated by cross-linking the proteins to DNA by adding 1% formaldehyde to the culture dishes for 10 min on a rocking platform at room temperature. The cross-linking was stopped with the addition of glycine solution. Cells were harvested and centrifuged for 10 min at 720 ×

g. Nrf2 antibody (2 μg each) was added to the pre-cleared chromatin in 0.65 ml siliconized tubes and incubated overnight on a rotator at 4 ℃. The oligonucleotide containing the Nrf2 binding site within the OGG1 promoter was obtained from Bioneer (Seoul, Republic of Korea). The ChIP procedure was analyzed using PCR with human OGG1 promoter-specific primers sense (−2192) 5'-CCTGGAAGAG-3' and antisense (–2078) 5'-AATGACTCTGGCG-3' and Platinum Taq High Fidelity (Invitrogen). The cycle parameters were as follows: first cycle at 95 ℃ for 5 min; 55 cycles at 95 ℃ for 30 s; 59 ℃ for 30 s; 72 ℃ for 30 s; and a final extension at 72 ℃ for 7 min. PCR products were resolved on a 1% agarose gel containing ethidium bromide, and visualized under UV illumination (Bartz et al., 2011).

2.10. Statistical analysis

All measurements were made in triplicate and all values are expressed as the means ± standard error of the mean (SEM). The results were subjected to an analysis of variance (ANOVA) using the Tukey test to analyze the significance of the difference. A probability of $p < 0.05$ was considered significant.

3. RESULTS

3.1. Effect of AgNPs on the transcriptional activity of the OGG1 promoter and on OGG1 mRNA and protein expression

The transcriptional activity of the OGG1 promoter was assessed using an OGG1 promoter linked to a luciferase reporter gene. AgNPs treatment (6-48 h) decreased the transcriptional activity of the OGG1 promoter in a time-dependent manner (Fig. 8A). The transcriptional activity of the OGG1 promoter in AgNPs-treated cells was consistent with the expression levels of OGG1 mRNA; AgNPs treatment decreased OGG1 mRNA levels in a time-dependent manner (6-48 h) (Fig. 8B). Similarly, the expression of OGG1 protein decreased in a time-dependent manner (6-48 h) in AgNPs-treated cells (Fig. 8C).

A
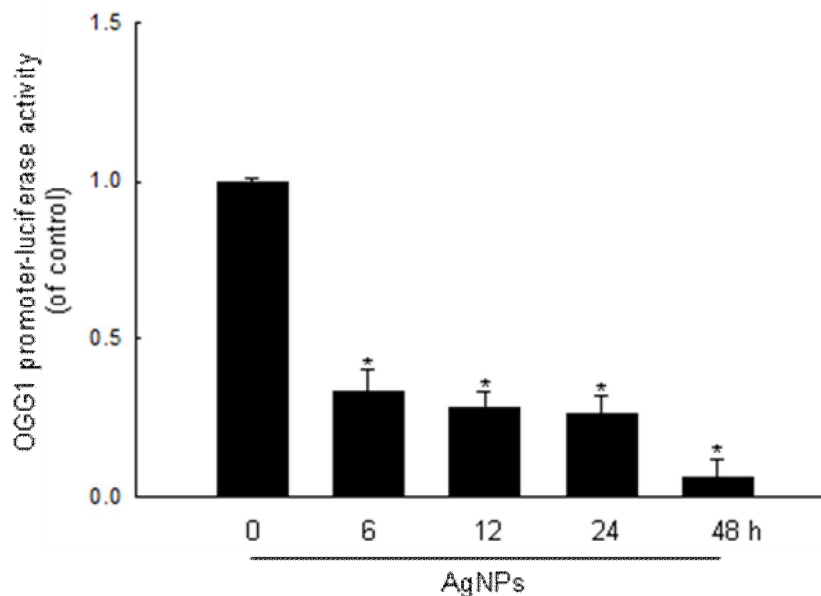
Fig. 8. Effect of AgNPs on transcriptional activity of OGG1 promoter, OGG1 mRNA expression and protein expression. (A) The time course of transcriptional activity of OGG1 promoter was measured after treatment of AgNPs at 4 μg/ml. *Significantly different from control ($p < 0.05$).

B
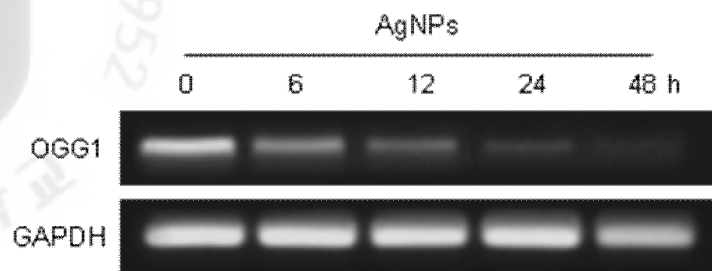
C
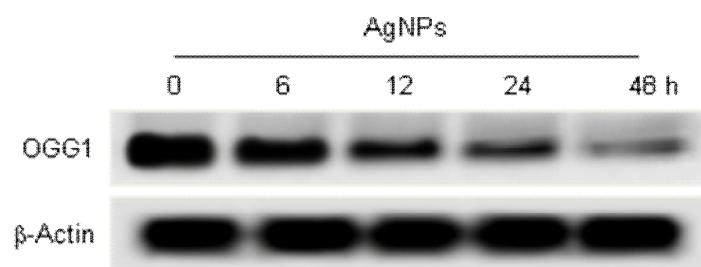
Fig. 8. continued. (B) OGG1 mRNA expression was analyzed by RT-PCR. (C) Cell lysates were electrophoresed and the expression of OGG1 protein was detected using an OGG1 specific antibody.

3.2. Effect of AgNPs on OGG1 activity

Confocal microscopic images showed that 8-oxoG-containing beacon-transfected control cells had fluorescence foci, indicating fluorescent cleavage bases containing 8-oxoG (Fig. 9A, right in upper panel). AgNPs treatment showed green fluorescence to be the inherent fluorescence of AgNPs in non-transfected control cells and 8-oxoG-containing beacon-transfected cells (Fig. 9A, left and right in lower panel). However, AgNPs treatment in 8-oxoG-containing beacon-transfected cells decreased the numbers of fluorescence foci compared to 8-oxoG-containing beacon-transfected control cells (Fig. 9A, right in lower and upper panel and histogram graph). The confocal microscopic data were consistent with the flow cytometric data (Fig. 9B).

A
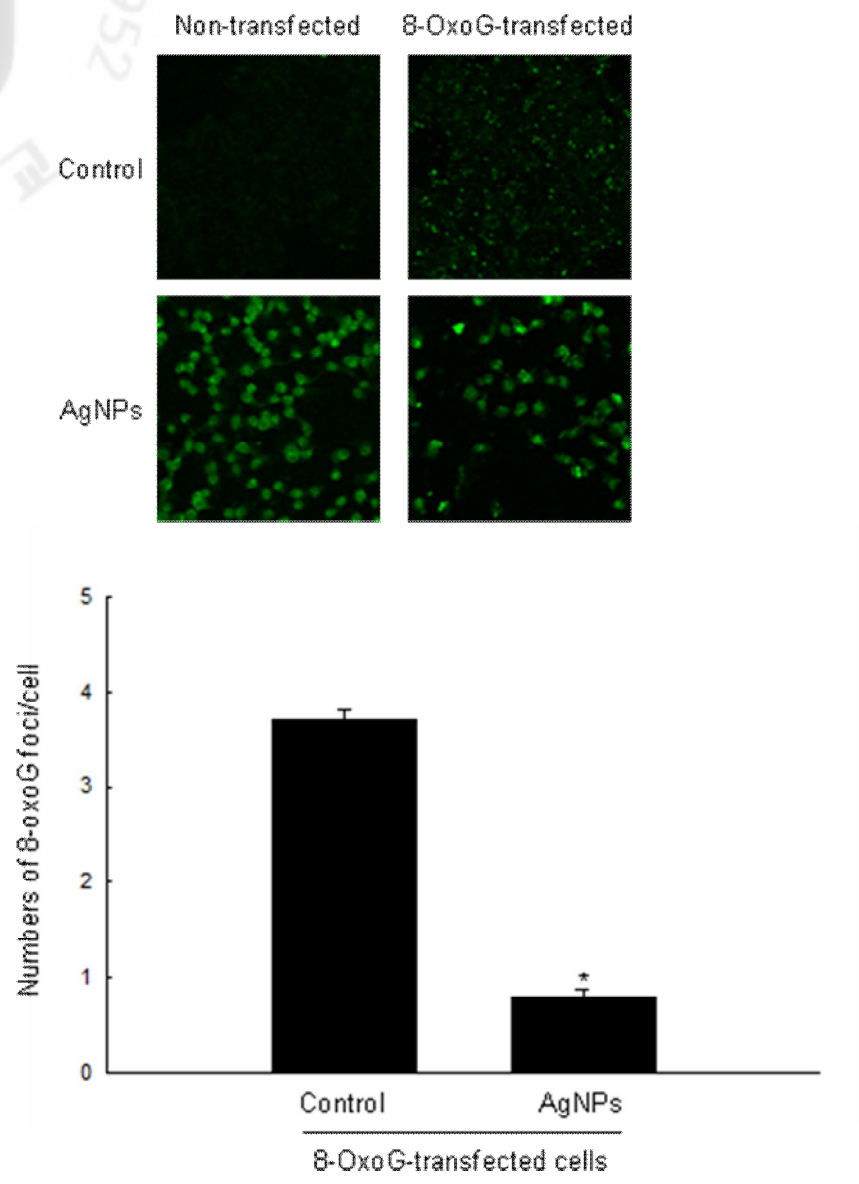
Fig. 9. Effect of AgNPs on OGG1 activity. The 8-oxoG-containing beacon was trans-fected

into cells. (A) The fluorescence foci of the cleaved bases containing 8-oxoG were detected by

confocal microscopy and counted. *Significantly different from control ($p < 0.05$).

B
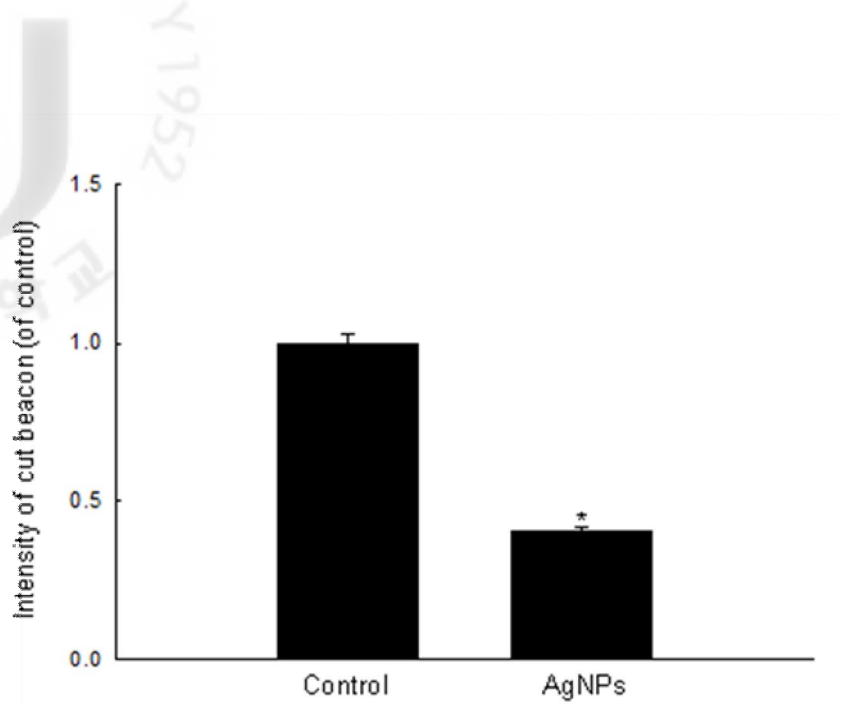
Fig. 9. continued. (B) The fluorescence foci were detected by flow cytometry. *Significantly different from control ($p < 0.05$).

3.3. Effect of AgNPs on the levels of 8-oxoG

The levels of 8-oxoG, a hallmark of oxidative stress-DNA base damage, were measured using an 8-OHdG detection kit and verified by immunochemistry. As shown in Fig. 10A, AgNPs increased the levels of 8-oxoG in DNA in a time-dependent manner (6-48 h). Condensed staining intensity of 8-oxoG was observed in AgNPs-treated cells (Fig. 10B). These results suggest that AgNPs increases the levels of 8-oxoG.

A
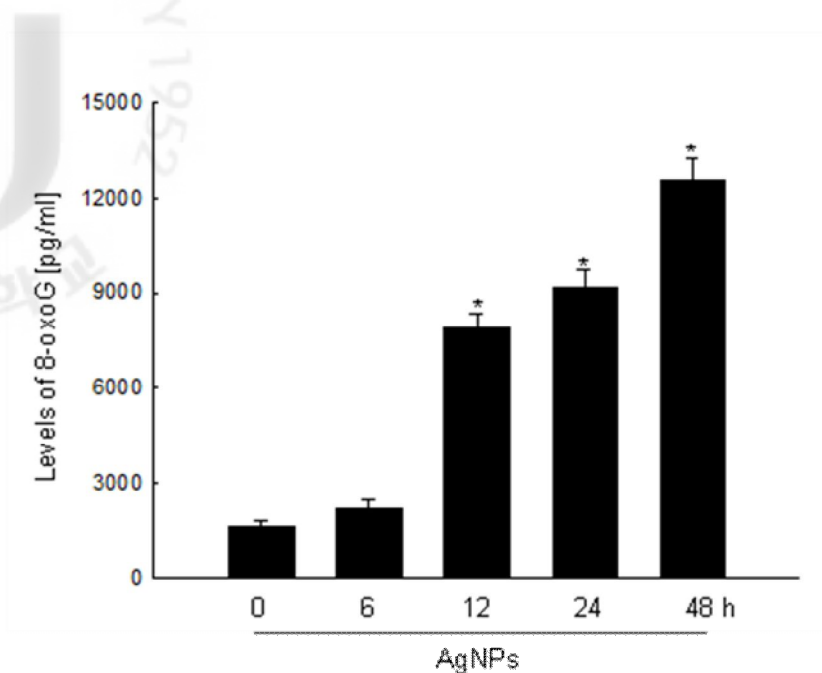
B
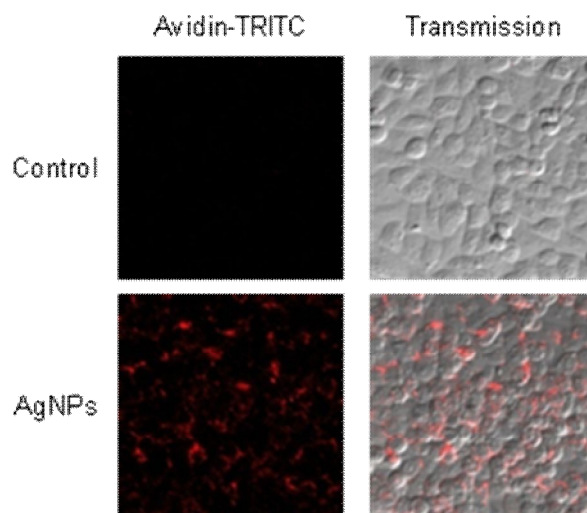
Fig. 10. Effect of AgNPs on 8-oxoG levels. (A) Cellular DNA was isolated using DNAzol reagent and the amount of 8-oxoG in DNA quantified using the Bioxytech 8-OHdG-ELISA kit. *Significantly different from control ($p < 0.05$). (B) 8-OxoG detected by the binding of avidin-TRITC conjugate was visualized by fluorescence microscope.

3.4. Effect of AgNPs on the Nrf2 transcription factor

   Nrf2 is an important transcription factor that regulates OGG1 gene expression. AgNPs

treatment resulted in decreased nuclear Nrf2 expression and translocation into the nucleus (Fig. 11A and B). As shown in Fig. 11B, AgNPs treatment changed the morphology of cells to round shape compared to control cells. In our previous report, AgNPs showed cytotoxicity via induction of apoptosis (Piao et al., 2011), suggesting that the morphological change in AgNPs-treated cells may be due to induction of apoptosis. Furthermore, AgNPs-treated cells exhibited almost no detectable Nrf2 binding to the sequence in OGG1 promoter (Fig. 11C).

A

B
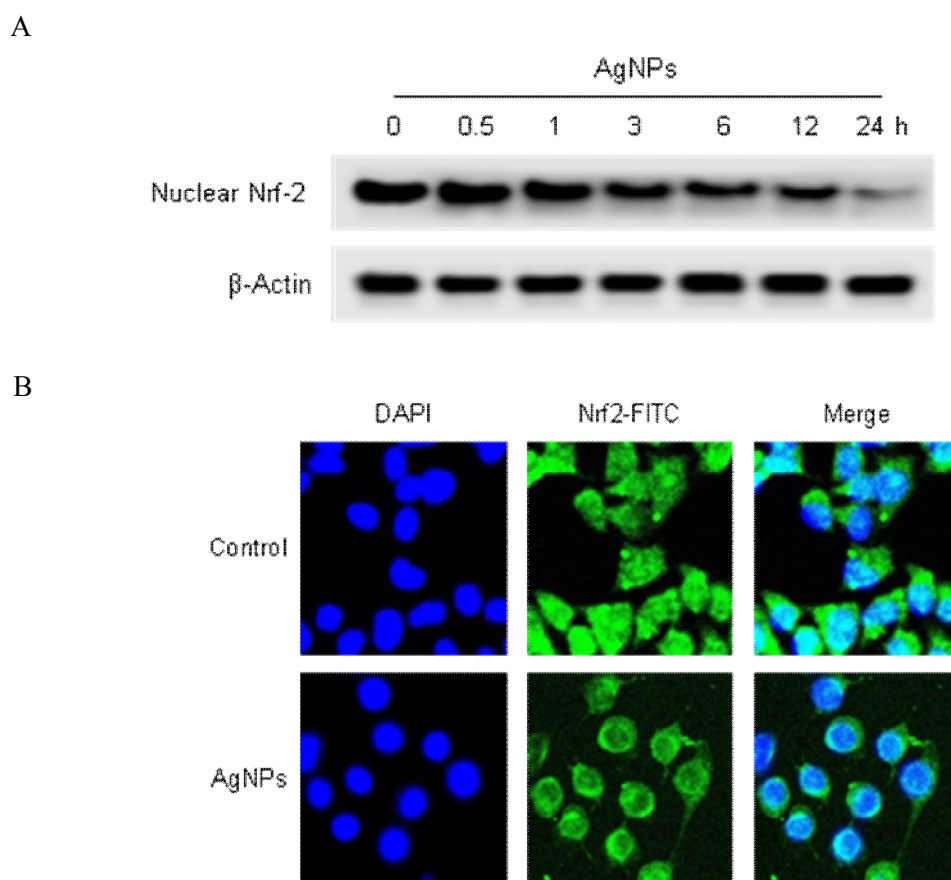
Fig. 11. Effects of AgNPs on Nrf2 expression, translocalization into the nucleus, and binding to OGG1 promoter. (A) Nuclear lysates were electrophoresed and the time-course of the effects of AgNPs on the expression of Nrf2 protein was detected using an Nrf2-specific antibody. (B) FITC-conjugated secondary antibody staining indi-cates the location of Nrf2 (green) by anti-Nrf2 antibody; DAPI staining indicates the location of the nucleus (blue); and the merged image indicates the nuclear location of Nrf2 protein.

C

IP : Nrf2

Control   AgNPs   Input

Nrf2 binding sequence
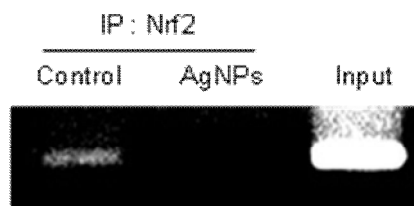
Fig. 11. continued. (C) Nrf2 binding sequence in OGG1 promoter obtained by the ChIP procedure was analyzed using PCR.

3.5. Effect of AgNPs on AKT and ERK

AKT and ERK1/2 are major signaling enzymes involved in cellular protection against oxidative stress and up-stream regulator of Nrf2. As shown in Fig. 12A and B, exposure to AgNPs caused a decrease in the phosphorylation (active form) of ERK1/2 and AKT in a time-dependent manner.

A

AgNPs

0   0.5   1   3   6   12   24 h

Phospho ERK1/2

ERK2

B

AgNPs

0   0.5   1   3   6   12   24 h

Phospho AKT

AKT
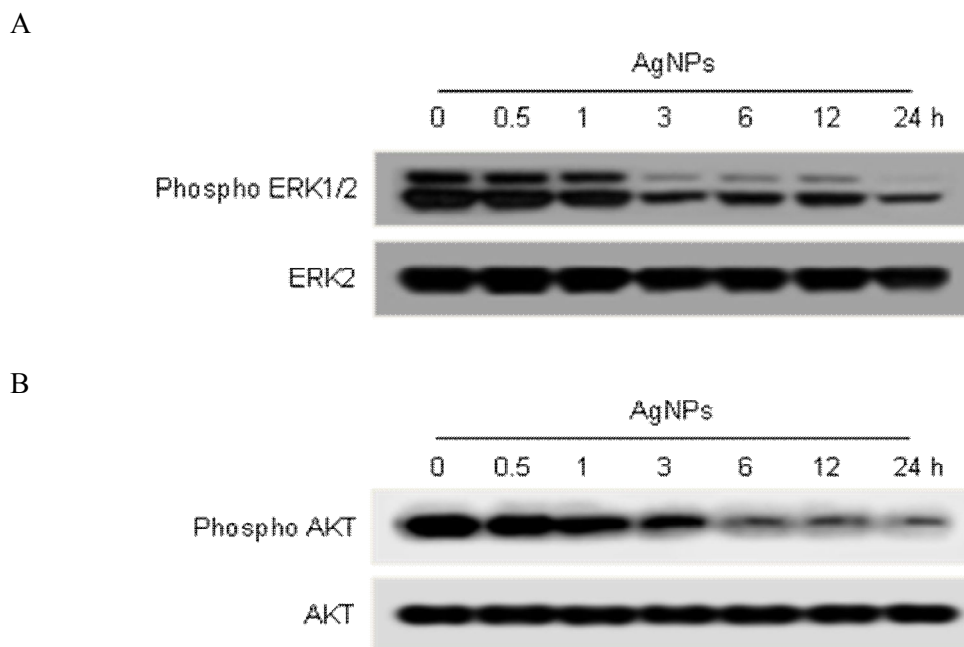
Fig. 12. Effect of AgNPs on the phosphorylation of AKT and ERK. Cell lysates were electrophoresed, and (A) phospho ERK1/2 and ERK2, (B) phospho AKT and AKT were detected by using their respective specific antibodies.

Collection @ jeju

4. DISCUSSION

Oxidative stress is caused by an imbalance between oxidants and antioxidants, and results in damage to membrane lipids, proteins and DNA, which leads to cell death (Toyokuni, 1999; Zimmerman, 1998; Ercal et al., 2001). Oxidative stress is an important mechanism mediating the toxicity of nanoparticles (Nel et al., 2006). For example, we recently reported that AgNPs induced ROS and damaged DNA, leading to apoptosis (Piao et al., 2011). 8-OxoG is known to be a sensitive marker of oxidative DNA damage (Shtarkman et al., 2008; Vadim et al., 2002), and is involved in mutagenesis, tissue/cell damage, and apoptosis (Hyun et al., 2000, 2003; Tsuzuki et al., 2007; Tsuruya et al., 2003). In the present study, AgNPs increased the levels of 8-oxoG in a time-dependent manner. This result demonstrated that oxidative stress induced by AgNPs causes DNA modification and leads to the accumulation of 8-oxoG in DNA.

OGG1 is a specific repair enzyme involved in the removal of 8-oxoG from DNA via the BER pathway in mammals, and plays an integral role in genomic maintenance. AgNPs decreased OGG1 activity, suggesting that inability of OGG1 to repair 8-oxoG leads to an increase of 8-oxoG in DNA. The inhibition of OGG1 activity by AgNPs could be the result of changes in gene transcription or translation. The transcriptional activity of OGG1 was decreased in AgNPs-treated cells and this led to a decrease in OGG1 mRNA expression. Similarly, OGG1 protein expression was decreased in AgNPs-treated cells. It has been suggested that the expression of OGG1 is affected by the redox status of the cell because a putative Nrf2 transcription factor binding site is present in the promoter of the human OGG1 (Dhénaut et al., 2000). In the present study, AgNPs down-regulated OGG1 expression by decreasing Nrf2 expression and Nrf2 binding to sequences present in the OGG1 gene promoter. Nrf2 is involved in the regulation of phase II xenobiotic metabolism and antioxidant genes, and is also an important factor in the inducible regulation of OGG1 (Cox, 2007). Structurally, Nrf2

is a basic leucine zipper transcription factor that under normal conditions remains sequestered in the cytosol (Moi et al., 1994; Venugopal and Jaiswal, 1998). Sequestration of Nrf2 is facilitated by interaction with its inhibitory partner, kelch-like protein 1 (Keap1) (Itoh et al., 1999; Dinkova-Kostova et al., 2002). Under basal conditions, Nrf2-Keap1 complexes are maintained in the cytosol tethered to the actin cytoskeleton where Nrf2 is continually targeted to the proteasome via an ubiquitin-dependent pathway (Nguyen et al., 2003). However, in the presence of ROS, xenobiotics or enzymatic activation, Nrf2 is released from Keap1 and translocates to the nucleus where it interacts with small Maf binding proteins. The final function of active Nrf2 is to interact with its cognate binding sequence in promoters and induce transcription (Itoh et al., 2004; Lee and Johnson, 2004; Nguyen et al., 2004). AgNPs decreases the nuclear level of Nrf2, its binding to its cognate sequence in the OGG1 promoter, and its transcriptional activity. The mechanisms leading to nuclear translocation of Nrf2 include its release from Keap1 in the cytosol. ERK and AKT phosphorylates Nrf2, which may facilitate the release of Nrf2 from the Keap1-Nrf2 complex, allowing activated Nrf2 to translocate into the nucleus where it forms a heterodimer with small Maf protein (Li et al., 2007; Chan et al., 2001; Kim et al., 2001; Kwak et al., 2002). Our data indicate that AgNPs act through down-regulation of ERK and AKT to down-regulate OGG1, resulting in the accumulation of oxidized DNA bases. The OGG1 promoter contains Nrf2 and stimulation protein-1 (SP-1) binding sites (Dhénaut et al., 2000). The AKT pathway regulates Nrf2 and SP-1 (Piantadosi et al., 2008; Sroka et al., 2007), and AKT up-regulation is involved in the resistance of cancer cells to gamma-ray via OGG1 induction (Ueta et al., 2008). ERK signaling regulates Nrf2 activation and ERK up-regulation involved in up-regulation of OGG1 against hyperoxic cytotoxicity (Papaiahgari et al., 2004; Kannan et al., 2006). Thus, the AKT and ERK pathways mediate up-regulation of OGG1. AKT and ERK have been implicated in the regulation of a variety of signal transduction pathways that mediate gene transcription, cell cycle events, cell

proliferation, DNA repair, and cell survival (Wanzel et al., 2005; Gao et al., 2004; Santos et al., 2001; Kandel et al., 2002; Yu et al., 2003; Ueta et al., 2008; Kannan et al., 2006).

In summary, 8-oxoG accumulation in AgNPs-treated cells occurs through decreased activities of ERK and AKT, decreased nuclear translocation of Nrf2, decreased Nrf2 binding to the OGG1 promoter, and down-regulation of OGG1 gene expression.

PART III

Silver nanoparticles induce cytotoxicity by the induction of reactive oxygen species levels and the attenuation of antioxidant enzymes via the inhibition of the AMPK-FOXO3 pathway

ABSTRACT

AgNPs-induced ROS generation and the resultant oxidative stress contribute to the cell damage associated with AgNPs. Recently, we reported that AgNPs induce oxidative cell damage accompanied by mitochondria-derived apoptosis. Antioxidant enzymes such as CAT and GPx have been reported to directly protect the cells from oxidative stress. In this study, we examined the roles of antioxidants in the high intracellular levels of ROS induced by AgNPs in human Chang liver cells and the molecular mechanisms involved. AgNPs increased ROS levels, coincided with the decreased expressions and activities of CAT and GPx and cell survival, but the addition of NAC, a potent antioxidant, significantly reduced the ROS levels, restored the activities of CAT and GPx, and finally abated cell deaths. AgNPs decreased an AMPK-FOXO3 pathway, which is a signal pathway for the induction of antioxidant enzymes. The AMPK activator (AICAR) significantly restored the expressions of CAT and GPx with the reduction of ROS levels and cytotoxicity, whereas the opposite changes were observed with an AMPK inhibitor (Compound C) and its specific siRNA. These results suggest that AgNPs-induced oxidative cytotoxicity might be at least partially attributed to the diminished antioxidant enzyme activities via the inhibition of the AMPK-FOXO3 pathway.

Keywords: Silver nanoparticles; Reactive oxygen species; Antioxidant enzyme; AMP-activated protein kinase; Forkhead transcription factor 3.

1. INTRODUCTION

AgNPs are clusters of silver atoms that range in diameter from 1 to 100 nm and are attracting interest as antibacterial and antimicrobial agents for applications in medicine (Chaloupka et al., 2010). Owing to their antibacterial properties, AgNPs have been used in various consumer products including textiles, personal care products, food storage containers, and laundry additives. Despite their widespread use, it has been reported that AgNPs accumulate in the liver and are associated with inflammatory, oxidative, genotoxic, and cytotoxic consequences (Johnston et al., 2010).
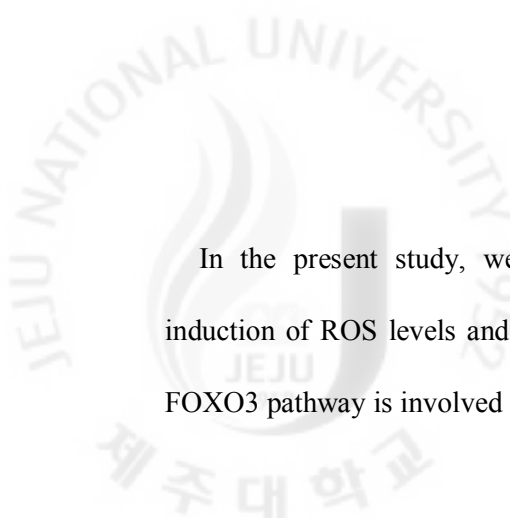
ROS are produced as a result of a wide range of environmental stimuli (Morel and Barouki, 1999). Excessive generation of ROS can cause cellular injury and dysfunction by directly oxidizing and damaging DNA, proteins, and lipids, as well as by activating several cellular stress-signaling and inflammatory pathways (Madamanchi and Runge, 2007). Understanding how ROS production and scavenging are regulated and developing strategies that reduce ROS production and increase antioxidant activity are important for preventing cytotoxicity (Jo et al., 2011). It is reported that the accumulation of AgNPs generates ROS and leads to cell death in cell systems (AshaRani et al., 2009; Foldbjerg et al., 2009). Recently, we reported that AgNPs cause cytotoxicity by oxidative stress-induced apoptosis and damage to cellular compounds (Piao et al., 2011).

Oxidative stress can lead to cell death, depending on the cell type and the level of oxidative insult (Bonfoco et al., 1995; Nicotera et al., 1997). Antioxidant enzyme systems are a well-developed regulatory mechanism protecting against oxidative stress. The detoxification of H_2O_2 (a highly ROS) in cells is predominantly mediated by the antioxidant enzymes CAT and GPx (Dringen et al., 2005; Liddell et al., 2006).

The CAT and GPx act as the primary antioxidants for ROS elimination before ROS

damage target cells (Briehl and Baker, 1996). Specially, increased CAT expression and activity have been shown to reduce intracellular ROS levels, resulting in resistance to oxidative stress-induced cell death (Shim et al., 2005). It has been reported that endogenous oxidative stress caused by the inhibition of CAT and GPx resulted in apoptosis in rat hepatocytes (Shiba and Shimamoto, 1999). Furthermore, it has been reported that the apoptosis induced by H_2O_2 in rat oligodendrocytes was potentiated by inhibiting CAT and GPx (Baud et al., 2004).

AMPK, an intracellular sensor of energy status, is activated to reserve cellular energy content. AMPK serves as a key regulator of cell survival or cell death in response to pathological stress such as oxidative stress, endoplasmic reticulum stress, hypoxia, and osmotic stress (Hayashi et al., 2000; Shin and Kim, 2009; Terai et al., 2005). AMPK deletion was reported to decrease the expression of CAT, superoxide dismutase (SOD), c-glutamylcystine synthase, and thioredoxine (Colombo and Moncada, 2009). Recent research has implicated GPx as a possible novel component of the antioxidant system that is enhanced by AMPK activation (Yun et al., 2009). This regulatory role is supported by increases in cell viability with treatment by the AMPK activators, including 5-aminoimidazole-4-carboxamide-1-β-D-ribofuranoside (Ido et al., 2002). Recent studies have found that FOXO3, one member in the FOXO family, is a direct downstream target of AMPK (Greer et al., 2007b). Increasing evidence suggests that AMPK can directly phosphorylate FOXO3 (T179, S399, S413, S555, S588, and S626), which mediates the ability of AMPK to reduce cell stress and to increase cell survival (Greer et al., 2007a; Greer et al., 2007b). The effects of FOXO3 are primarily mediated via the up-regulated transcription of CAT and GPx (Marinkovic et al., 2007; Nemoto and Finkel, 2002). Although the biological effects of AgNPs have been diversely studied, it is not yet clear whether the cytotoxicity effect of ROS is mediated by AMPK pathway.

In the present study, we examined whether AgNPs increase the cytotoxicity by the induction of ROS levels and the inhibition of antioxidant enzymes, and whether the AMPK-FOXO3 pathway is involved in the regulation of antioxidant enzymes.

2. MATERIALS AND METHODS

2.1. Reagents

AgNPs were provided by Professor Jinhee Choi of Seoul University (Seoul, Repubilc of Korea), which were characterized as described previously (Eom and Choi, 2010). DCF-DA, NAC, MTT, β-actin antibody and 5-Aminoimidazole-4-carboxamide-1-β-D-ribofuranosyl 5′-monophosphate (AICAR) were purchased from Sigma Chemical Company (St. Louis, MO, USA). The primary CAT and GPx antibodies were purchased from Santa Cruz Biotechnology (Delaware Avenue, CA, USA). Phospho AMPKα (Thr 172), AMPKα, FOXO3 antibodies were purchased from Cell Signaling Technology (Beverly, MA, USA). Phospho serine/phospho threonine antibody was purchased from Abcam (Cambridge, MA, USA). Compound C was provided by Calbiochem (San Diego, CA, USA). The other chemicals and reagents were of analytical grade.

2.2. Cell culture

Human Chang liver cells were obtained from the American type culture collection (Rockville, MD, USA) and maintained at 37 ℃ in an incubator with a humidified atmosphere of 5% CO_2 and cultured in RPMI-1640 medium containing 10% heat-inactivated fetal calf serum, streptomycin (100 μg/ml) and penicillin (100 U/ml).

2.3. Western blot analysis

Cells were lysed on ice for 30 min in 100 μl of a lysis buffer (120 mM NaCl, 40 mM Tris pH 8.0, 0.1% NP 40) and were centrifuged at 13,000 × g for 15 min. The supernatants were collected from the lysates and the protein concentrations were determined. Aliquots of the lysates (40 μg of protein) were boiled for 5 min and were electrophoresed in 10% SDS-

polyacrylamide gel. The proteins in the gels were transferred onto nitrocellulose membranes (Bio-Rad, Hercules, CA, USA), and were subsequently incubated with primary antibodies. The membranes were further incubated with secondary anti-immunoglobulin-G-horseradish peroxidase conjugates (Pierce, Rockford, IL, USA), followed by exposure to X-ray film. The protein bands were detected using an enhanced chemiluminescence western blotting detection kit (Amersham, Little Chalfont, Buckinghamshire, UK).

2.4. CAT activity

Cells were seeded at 1×10^5 cells/ml, and at 16 h after plating, cells were treated with AgNPs at 4 μg/ml for 0.5 to 24 h. The harvested cells were suspended in 10 mM phosphate buffer (pH 7.5) and were then lysed on ice by sonication twice for 15 sec. Triton X-100 (1%) was then added to the lysates, which were further incubated for 10 min on ice. The lysates were centrifuged at $5,000 \times g$ for 30 min at 4 ℃ to remove cellular debris, and the protein content was determined. For detection of CAT activity, 50 μg of protein was added to 50 mM of phosphate buffer (pH 7) containing 100 mM of H_2O_2. The reaction mixture was incubated for 2 min at 37 ℃, and the absorbance was monitored at 240 nm for 5 min. The changes in absorbance with time were proportional to the breakdown of H_2O_2. The CAT activity was expressed as U/mg protein where 1 U of enzyme activity was defined as the amount of enzyme required to breakdown of 1 μM of H_2O_2 (Carrillo et al., 1991).

2.5. GPx activity

For the detection of GPx activity, 50 μg of the protein was added to 25 mM phosphate buffer (pH 7.5) containing 1 mM EDTA, 1 mM NaN_3, 1 mM glutathione, 0.25 unit of glutathione reductase, and 0.1 mM NADPH. After incubation for 10 min at 37 ℃, H_2O_2 was added to the reaction mixture at a final concentration of 1 mM. The absorbance was monitored

at 340 nm for 5 min. The GPx activity was measured as the rate of NADPH oxidation by change in absorbance at 340 nm (Paglia and Valentine, 1967). The GPx activity was expressed as U/mg protein and one unit of enzyme activity was defined as the amount of enzyme required to oxidize 1 mM NADPH.

2.6. Intracellular ROS measurement

Cells were treated with AgNPs and were incubated for various times at 37 ℃. After adding 25 μM of DCF-DA solution, the fluorescence of 2′,7′-dichlorofluorescein was detected using a Perkin Elmer LS-5B spectrofluorometer and a flow cytometer (Becton Dickinson, Mountain View, CA, USA) (Rosenkranz et al., 1992). The image analysis for the generation of intracellular ROS was achieved by seeding the cells on a cover slip-loaded six well plate at 2×10^5 cells/well. Sixteen hours after plating, cells were treated with AgNPs. Thirty minutes later, 100 μM of DCF-DA was added to each well, and cells were incubated for an additional 30 min at 37 ℃. After washing with PBS, the stained cells were mounted onto a microscope slide in mounting medium (DAKO, Carpinteria, CA, USA). The microscopic images were collected using the Laser Scanning Microscope 5 PASCAL program (Carl Zeiss, Jena, Germany) on a confocal microscope.

2.7. Cell viability

Cells were treated with AgNPs for 24 h, and 50 μl of the MTT stock solution (2 mg/ml) was added to each well to reach a total reaction volume of 200 μl. After incubating for 4 h, the plate was centrifuged at $800 \times g$ for 5 min followed by aspiration of the supernatants. The formazan crystals in each well were dissolved in 150 μl of dimethylsulfoxide, and the A_{540} was read on a scanning multi-well spectrophotometer (Carmichael et al., 1987). To determine the effect of the AMPK pathway on cell viability, cells were pre-treated with 1 mM of AICAR (an

Collection @ jeju

activator of AMPK) for 1 h, and 2 μM of Compound C (an inhibitor of AMPK) for 1 h, followed by AgNPs for 24 h. The cell viability was measured using the MTT assay.

2.8. Immunoprecipitation and Western blot analysis for the detection of phosphorylated FOXO3

FOXO3 was immunopreciptated from the nuclear extracts using FOXO3 antibody. Immune complexes were collected with protein G beads and were washed with immunoprecipitation buffer. Equal amounts of precipitates were run on a SDS-polyacrylamide gel, and Western blotting was performed with antibody specific to phospho serine/phospho threonine (Amos et al., 2005).

2.9. Transient transfection of siRNA

Cells were seeded at 1.5×10^5 cells/well in 24 well plate and allowed to reach approximately 50% confluence on the day of transfection. The siRNA construct used were mismatched siRNA Control (Santa Cruz Biotechnology, Santa Cruz, CA) and siRNA AMPK (Bioneer Corporation, Bioneer, Repubilc of Korea). Cells were transfected with 10-50 nM siRNA using lipofectamine^{TM} 2000 (Invitrogen, Carlsbad, CA) according to the manufacturer's instruction. At 24 h after transfection, cells were treated with AgNPs for 1 or 24 h and examined by DCF-DA and MTT assay.

2.10. Statistical analysis

All measurements were made in triplicate and all values were expressed as the means ± standard error of the mean (SEM). The results were subjected to an analysis of variance (ANOVA) using the Tukey test to analyze the difference. A $p<0.05$ was considered significant.

3. RESULTS

3.1. AgNPs induced ROS generation, decreased intracellular antioxidant enzymes, and cell viability

In our previous results, AgNPs showed IC_{50} (concentration yielding 50% growth inhibition) about 4 μg/ml (Piao et al., 2011). The concentration of AgNPs corresponding to the IC_{50} was used as optimal concentration for further study. Oxidative stress has been cited to be one of the more important mechanisms of toxicity related to nanoparticle exposure (Nel et al., 2006). To investigate the potential role of oxidative stress by AgNPs, the generation of ROS was measured. As shown in Fig. 13A, the ROS levels generated by AgNPs were maintained until 24 h, and AgNPs-induced ROS were suppressed by NAC, a synthetic antioxidant. This pattern was also confirmed by confocal microscopy image that the red fluorescence intensity of ROS was enhanced in AgNPs-treated cells compared to control cells. NAC reduced the fluorescence intensity of DCF-DA in AgNPs-treated cells (Fig. 13B). The protein expressions and activities of CAT and GPx in AgNPs-treated cells were measured. As shown in Fig. 13C, AgNPs at 4 μg/ml decreased the protein expressions of CAT and GPx in a time-dependent manner (0.5 to 24 h). In addition, AgNPs also decreased the activities of CAT and GPx in a time-dependent manner as shown in Fig. 13D. To investigate whether the AgNPs-generated ROS levels affected the activities of antioxidant enzymes, NAC was treated for 1 h prior to treatment with AgNPs, and CAT and GPx activities were determined after 1 h incubation. As shown in Fig. 13E, NAC pretreatment dramatically suppressed AgNPs-attenuated antioxidant enzymes activities. Further NAC was found to prevent AgNPs-induced cytotoxicy (Fig. 13F). Taken together, these results suggest that AgNPs decreased the protein expression and activities of CAT and GPx and cell viability in AgNPs-treated cells may be due to induction of ROS.
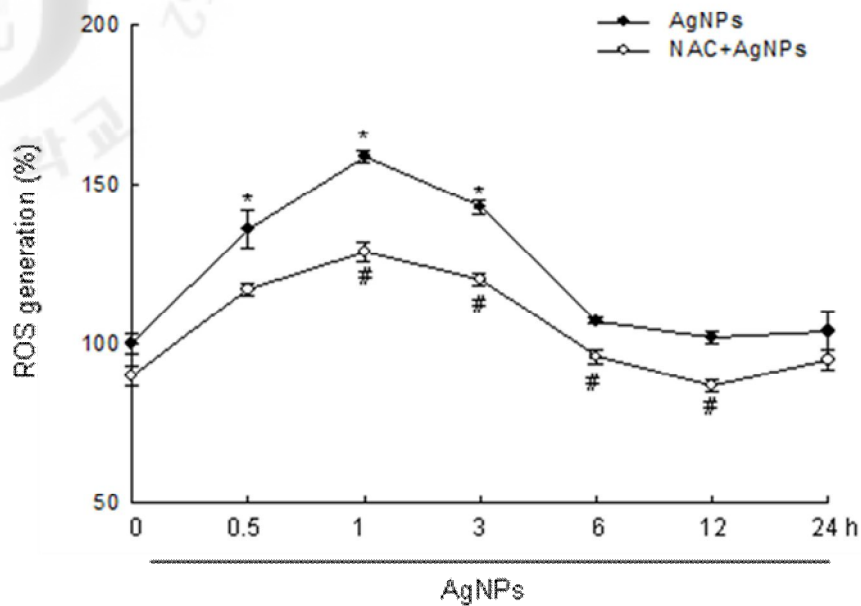
Fig. 13. Time course of AgNPs on intracellular ROS, protein expressions and activities of CAT and GPx, and cytotoxicity in Chang liver cells. Cells were treated with NAC at 2 mM. After 30 min, 4 μg/ml of AgNPs was added to the plate at indicated times (0.5 to 24 h). The intracellular ROS level was detected by spectrofluorometry (A) after the DCF-DA treatment. The values were expressed as means ± SEM. *significantly different from control ($p < 0.05$), and #significantly different from AgNPs-treated cells ($p < 0.05$).

B

| Control | NAC | AgNPs | NAC+AgNPs |
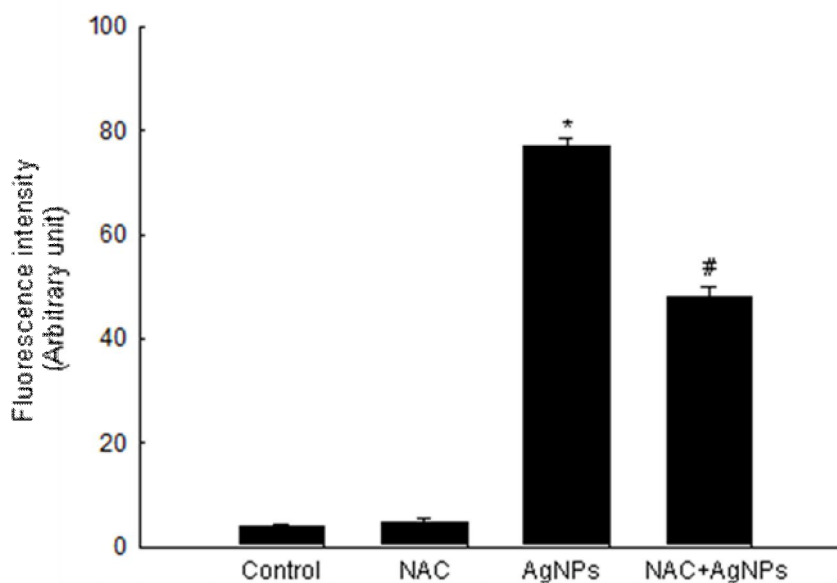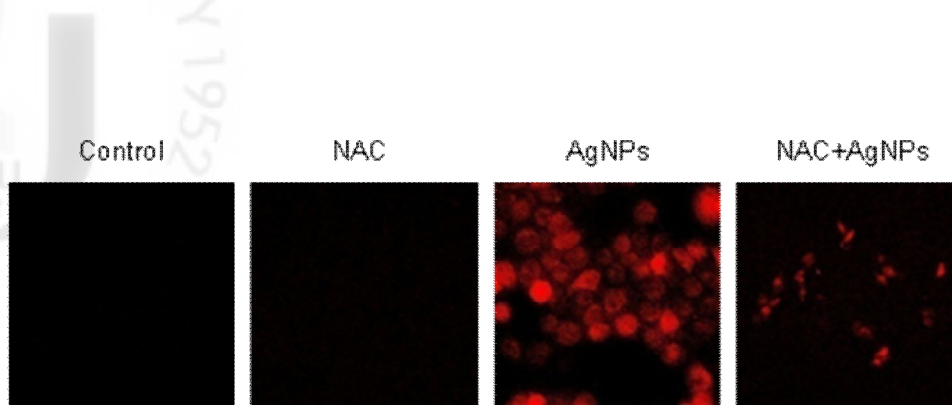
Fig. 13. continued. (B) The representative confocal images illustrate the increase in red fluorescence intensity of DCF produced by ROS in AgNPs-treated cells compared to the control and indicate the lowered fluorescence intensity in AgNPs-treated cells with NAC (original magnification×400). Histogram graph of fluorescence intensity indicates *significantly different from control ($p < 0.05$), and #significantly different from AgNPs-treated cells ($p < 0.05$).

C
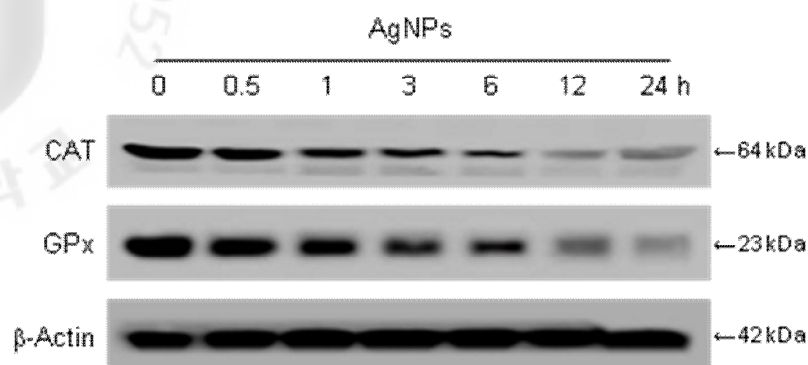
D
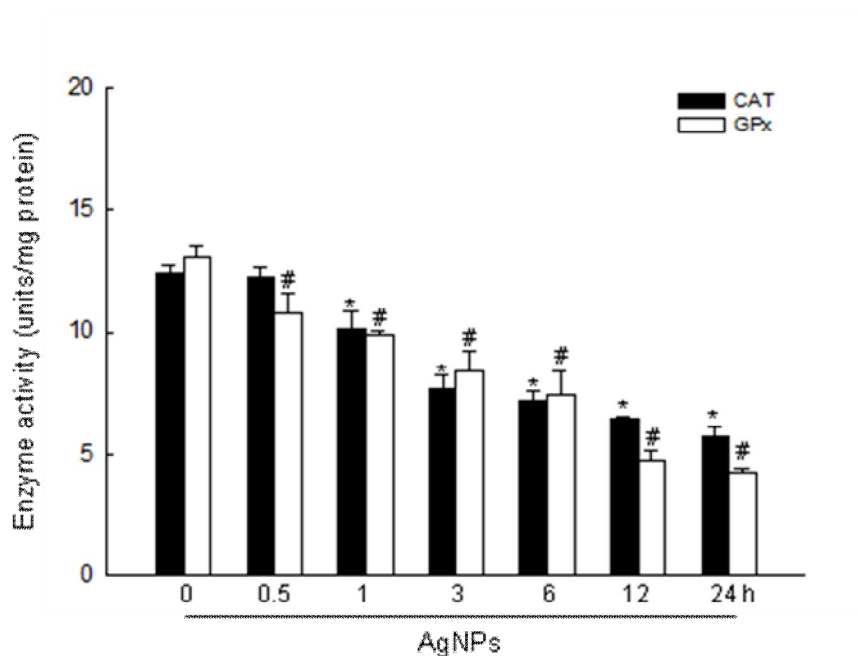
Fig. 13. continued. (C) Western blot analysis was performed using CAT and GPx antibodies. (D) The activities of CAT and GPx are expressed as means (U/mg protein) ± SEM. *Significantly different from control cells in CAT activity, and #significantly different from control cells in GPx activity.

E
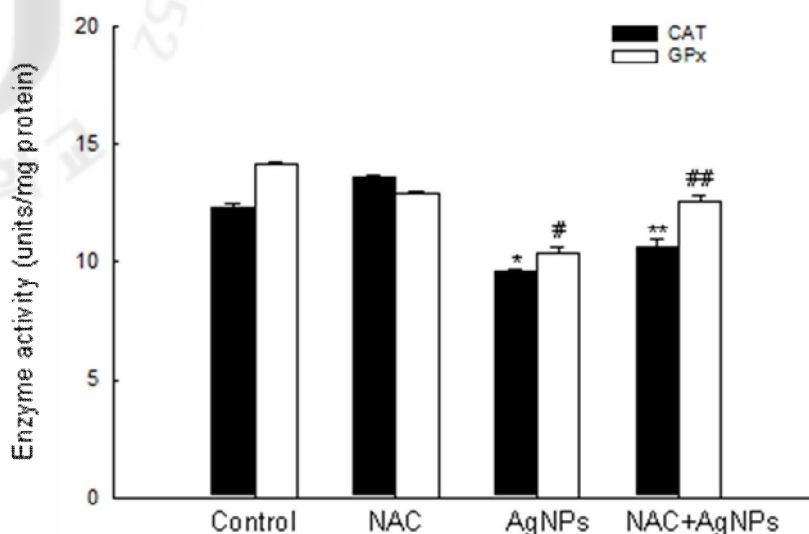
F
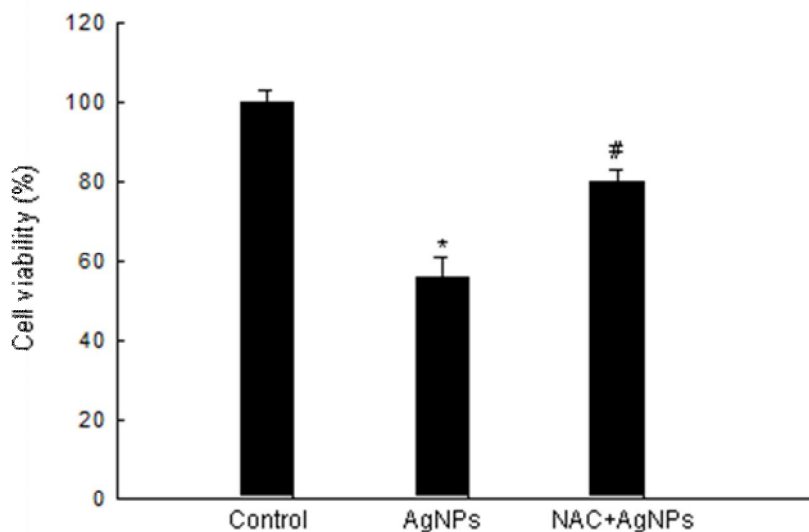
Fig. 13. continued. (E) NAC was treated for 1 h prior to treatment with AgNPs, and CAT and GPx activities were determined after 1 h incubation. *Significantly different from control cells, and **significantly different from AgNPs-treated cells in CAT activity ($p < 0.05$). #Significantly different from control cells, and ##significantly different from AgNPs-treated cells in GPx activity ($p < 0.05$). (F) Cells were treated with AgNPs at 4 μg/ml for 24 h, and cytotoxicity was determined by measuring MTT method. *Significantly different from control ($p < 0.05$), and #significantly different from AgNPs-treated cells ($p < 0.05$).

3.2. AgNPs decreased AMPK signaling pathway

Recent papers showed that AMPK has cell protection against ROS (Li et al., 2009) and FOXO3 was identified as a downstream target of AMPK (Greer et al., 2007b). To define the mechanism involved in the protective effect of antioxidant enzyme, cells were treated with AgNPs for up to 24 h. The phospho AMPK (active form of AMPK) in AgNPs-treated cells was decreased in a time dependent manner (from 0.5 h to 24 h) (Fig. 14A). Accordingly, the phospho FOXO3 (active form of FOXO3) in AgNPs-treated cells was decreased in a time dependent manner (Fig. 14B). These results suggest that AgNPs regulated the AMPK-FOXO3 signaling pathway.

A
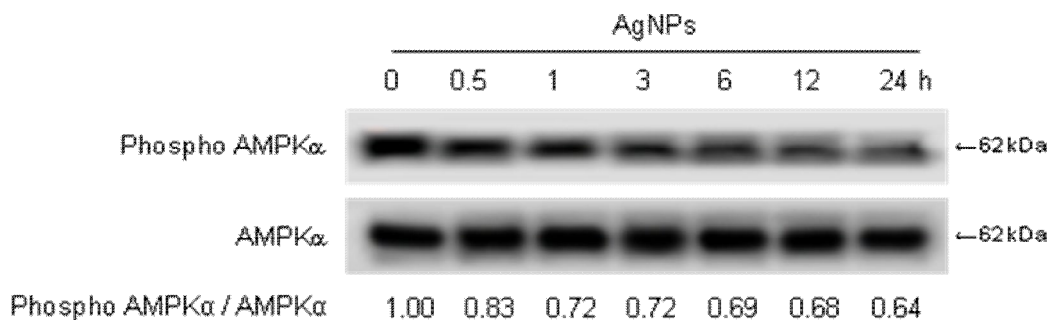
B
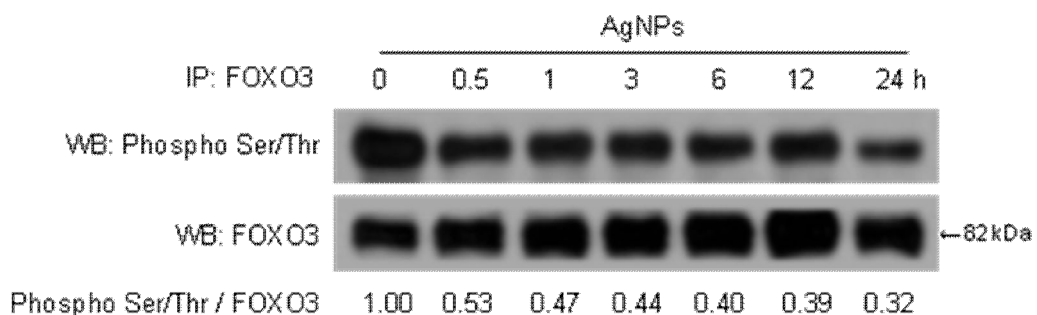
Fig. 14. Effects of AgNPs on AMPK signaling pathway. (A) Active form of AMPK was performed by Western blot analysis using phospho AMPK antibody. (B) Cell lysates were immunoprecipitated with FOXO3 antibody, and precipitates were Western blotted with antibodies against phospho serine/phospho threonine and FOXO3.

3.3. AMPK activator modulates AgNPs-induced ROS generation, cytotoxicity, and antioxidant enzyme expression

Previous studies have shown that the activation of the AMPK pathway reduces intracellular ROS levels (Ceolotto et al., 2007; Kukidome et al., 2006; Ouedraogo et al., 2006; Zhang et al., 2008). To further elucidate the AMPK-FOXO3 pathway involved in AgNPs-induced ROS generation and the inhibition of the antioxidant enzyme, AMPK activator (AICAR) was examined for its the effects on ROS, CAT and GPx. The fluorescence spectrometric data revealed that AgNPs treatment increased the level of ROS compared to the control. However, AICAR at 1 mM treatment attenuated the AgNPs-induced ROS increase (Fig. 15A).

A
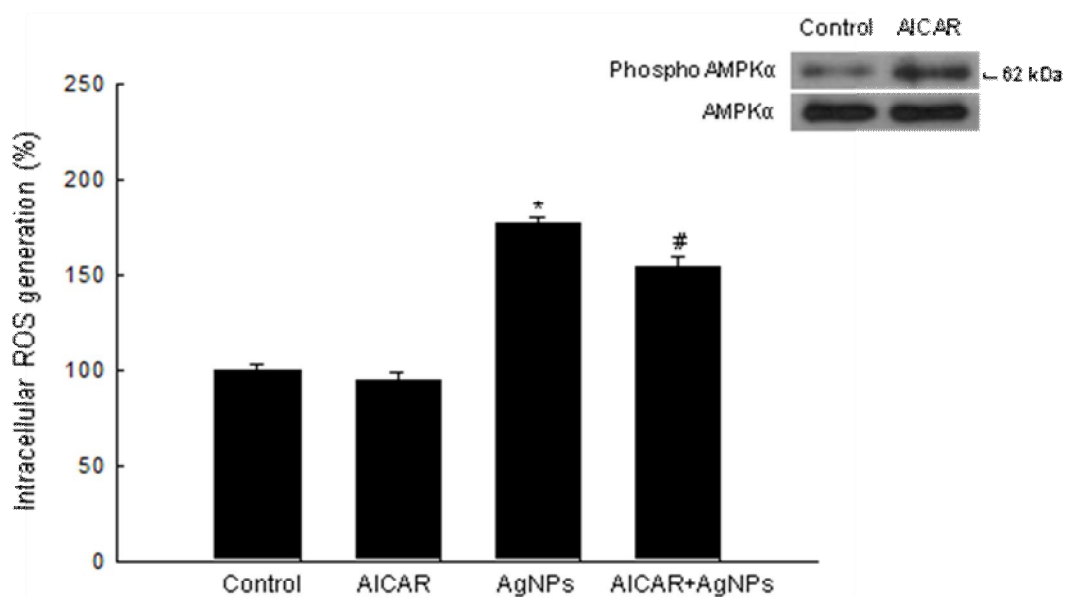
Fig. 15. Effects of AMPK activator on ROS generation, cytotoxicity, CAT and GPx expression in AgNPs-treated cells. (A) Cells were treated with AICAR at 1 mM. After 30 min, 4 μg/ml of AgNPs was added to the plate. After an additional 1 h, the intracellular ROS level was detected by spectrofluorometry after the DCF-DA treatment. *Significantly from control ($p < 0.05$), and #significantly from AgNPs-treated cells ($p < 0.05$).

An analysis of confocal microscope data revealed that AICAR reduced the red fluorescence intensity of AgNPs-induced intracellular ROS as shown in Fig. 15B. In addition, pre-treatment with AICAR attenuated AgNPs-induced cytotoxicity (Fig. 15C). AICAR treatment rescued the expressions of CAT and GPx that were decreased by AgNPs (Fig. 15D).

B
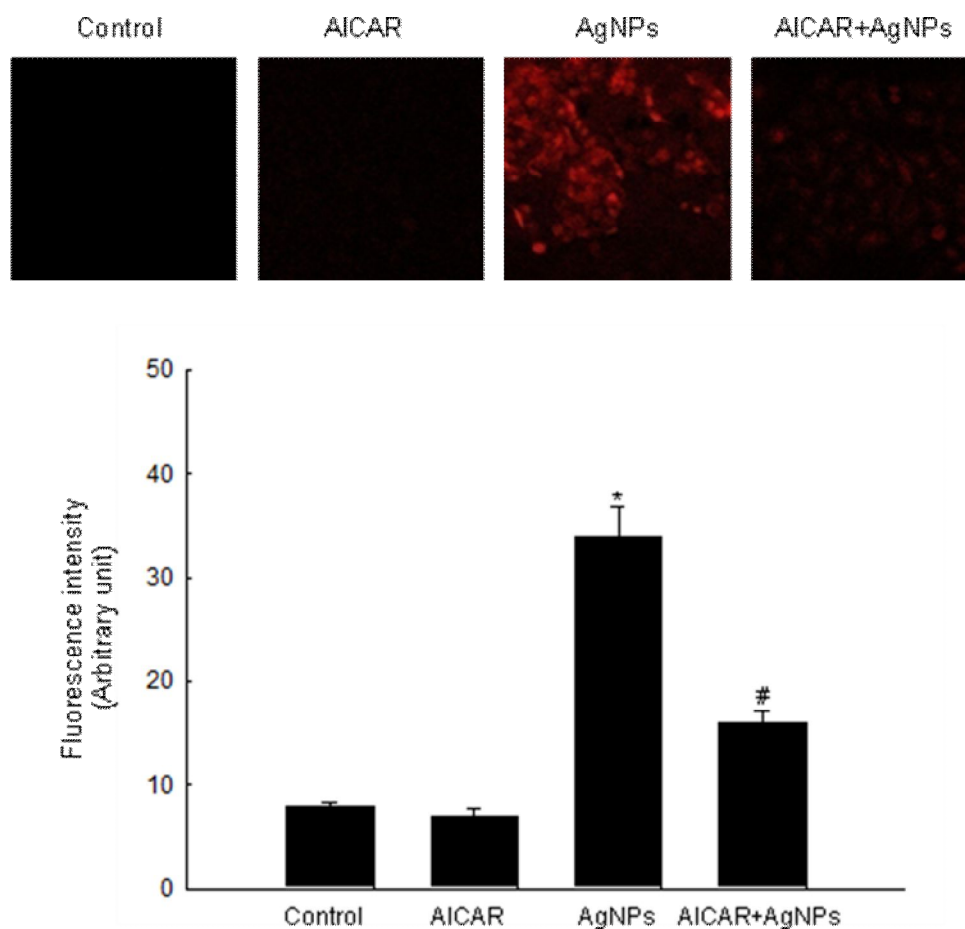
Fig. 15. continued. (B) The representative confocal images illustrate the increase in red fluorescence intensity of DCF produced by ROS in AgNPs-treated cells compared to the control and indicate the lowered fluorescence intensity in AgNPs-treated cells with AICAR (original magnification×400). Histogram graph of fluorescence intensity indicates *significantly different from control ($p < 0.05$), and #significantly different from AgNPs-treated cells ($p < 0.05$).

C
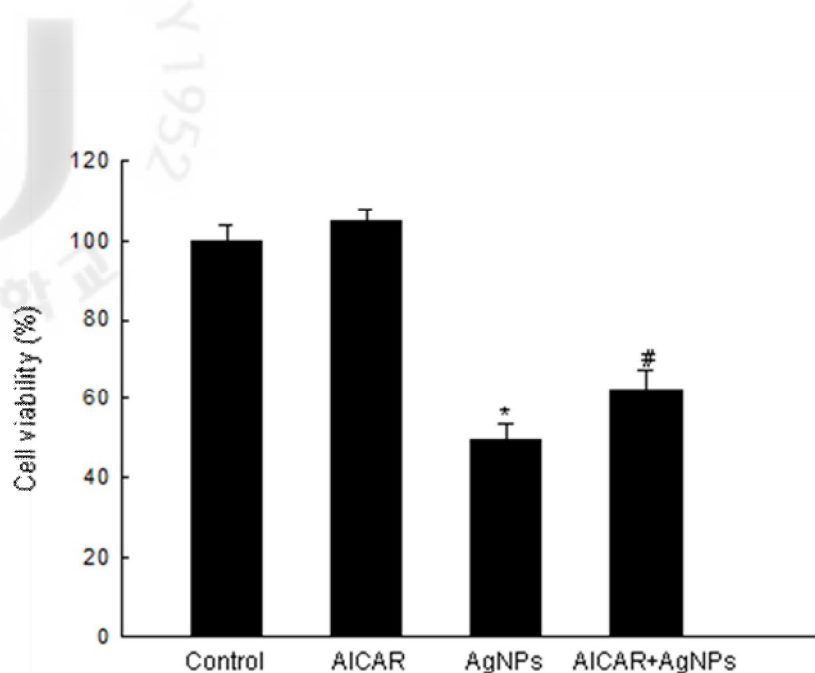
D
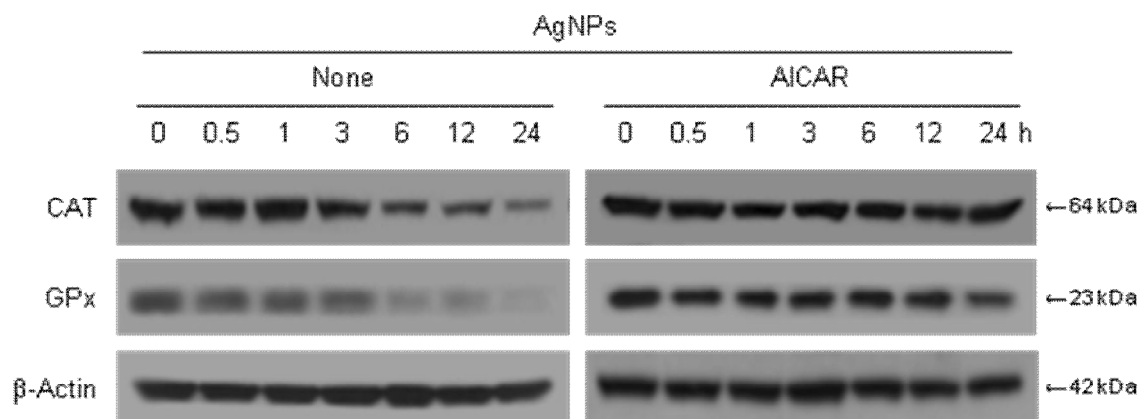
**Fig. 15. continued.** (C) Cells were treated with AgNPs for 24 h, and cell viability was determined by measuring MTT method. *Significantly from control ($p < 0.05$), and #significantly from AgNPs-treated cells ($p < 0.05$). (D) Western blot analysis was performed using CAT and GPx antibodies in AgNPs-treated cells and AgNPs-treated cells with AICAR.

3.4. Suppression of AMPK regulates AgNPs-induced ROS generation, cytotoxicity, and antioxidant enzyme expression

To confirm the role of AMPK on AgNPs-mediated ROS generation, cytotoxicity, and antioxidant enzyme expression, AMPK inhibitor (Compound C) and siRNA AMPK were used in this study. The fluorescence spectrometric data revealed that Compound C at 2 μM treatment enhanced the AgNPs-induced ROS increase (Figs. 16A and B). Pre-treatment with Compound C increased AgNPs-induced cytotoxicity (Fig. 16C) and further reduced the expressions of CAT and GPx that were decreased by AgNPs (Fig. 16D). In addition, knockdown of AMPK markedly enhanced ROS generation and cytotoxicity (Figs. 17A and B).

A
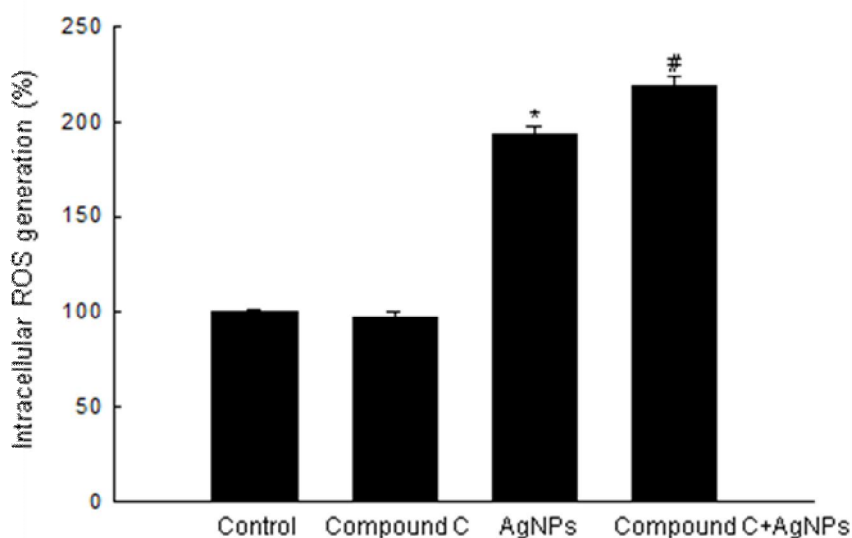
**Fig. 16.** Effects of AMPK inhibitor on ROS generation, cytotoxicity, CAT and GPx expressions in AgNPs-treated cells. (A) Cells were treated with Compound C at 2 μM. After 30 min, AgNPs was added to the plate. After an additional 1 h, the intracellular ROS was detected by spectrofluorometry after the DCF-DA treatment. *Significantly from control ($p < 0.05$), and #significantly from AgNPs-treated cells ($p < 0.05$).

B
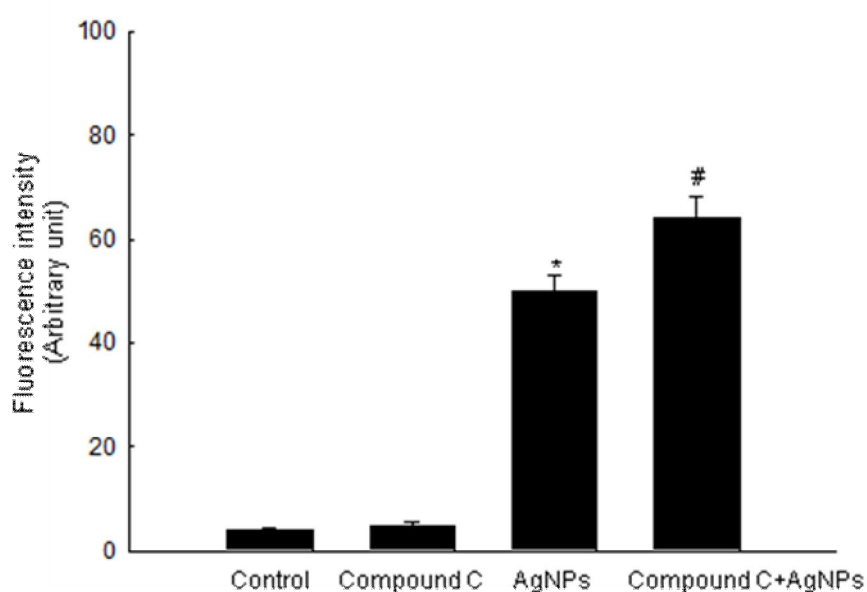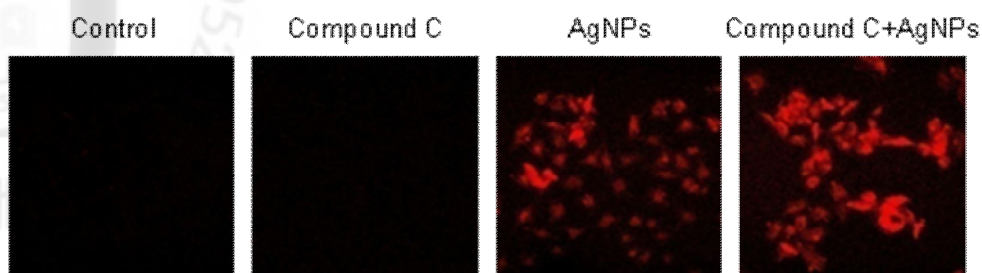
Fig. 16. continued. (B) The representative confocal images illustrate the increase in red fluorescence intensity of DCF produced by ROS in AgNPs-treated cells with Compound C compared to the intensity in AgNPs-treated cells (original magnification×400). Histogram graph of fluorescence intensity indicates *significantly different from control ($p < 0.05$), and #significantly different from AgNPs-treated cells ($p < 0.05$).

C
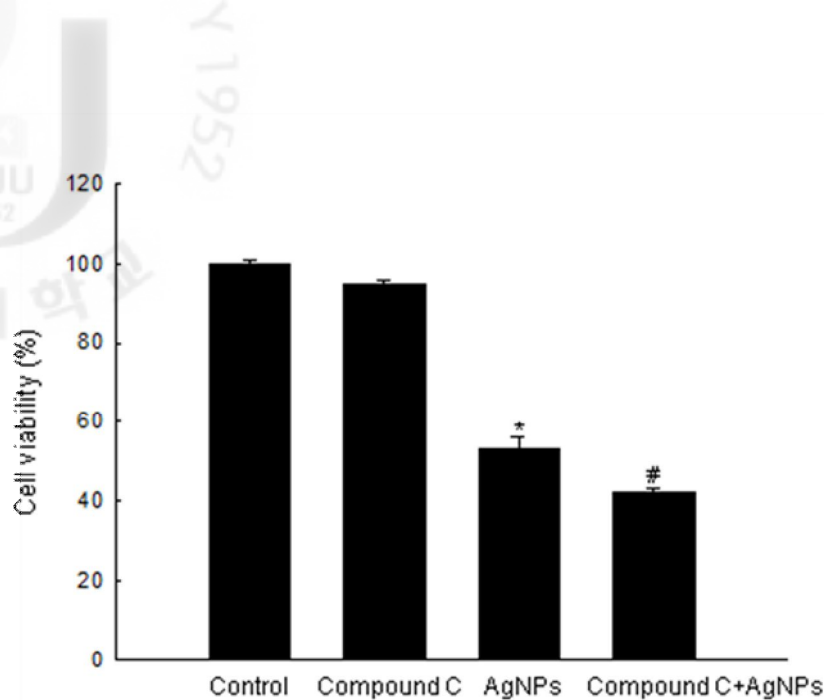
D
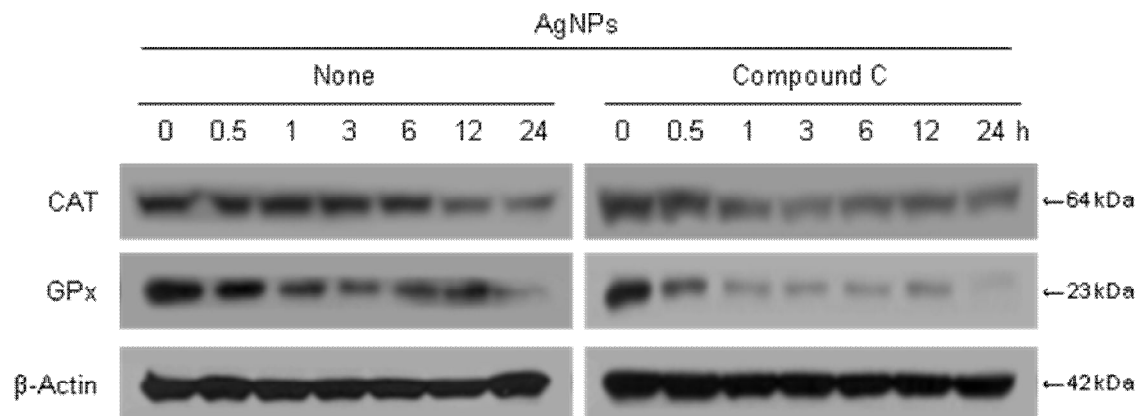
Fig. 16. continued. (C) Cells were treated with AgNPs for 24 h, and cytotoxicity was determined by measuring MTT method. *Significantly from control ($p < 0.05$), and #significantly from AgNPs-treated cells ($p < 0.05$). (D) Western blot analysis was performed using CAT and GPx antibodies in AgNPs-treated cells and AgNPs-treated cells with Compound C.
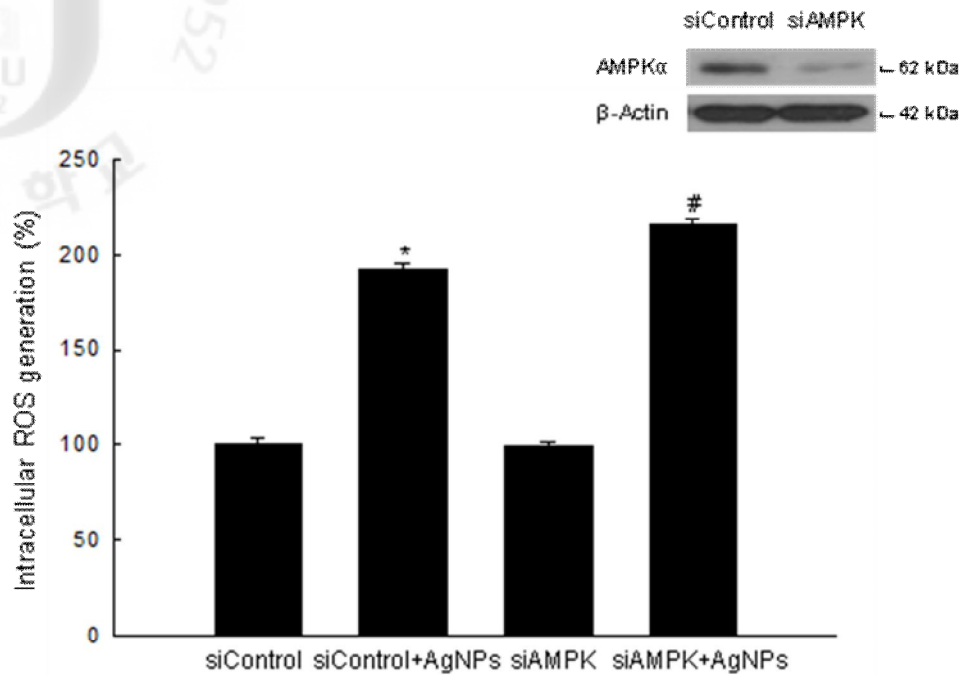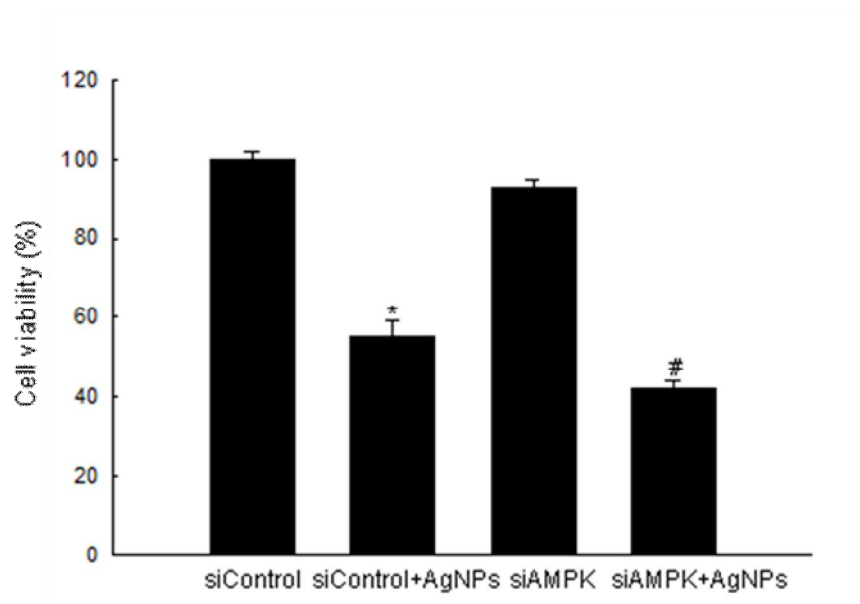
Fig. 17. Knockdown of AMPK on ROS generation and cytotoxicity in AgNPs-treated cells. Human Chang liver cells were transfected with control or AMPK siRNA, and intracellular ROS and cell viability were detected by DCF-DA and MTT, respectively. *Significantly different from control ($p < 0.05$), and #significantly different from AgNPs-treated cells ($p < 0.05$).

4. DISCUSSION

In the present study, we showed that AgNPs induce cytotoxicity by the induction of ROS and inhibition of the antioxidant enzymes CAT and GPx via the down-regulation of AMPK-FOXO3 pathway. Characterization of used AgNPs in this study as described previously showed that the particle size of AgNPs has an even distribution, with 5-10 nm, and tend to agglomerate when expose to cells, exhibiting that the main particle sizes distributed in the medium were about 28-35 nm, and be up-taken by cells (Eom and Choi, 2010). We have previously proved that AgNPs showed cytotoxicity, which was higher than $AgNO_3$, in a dose-dependent manner in human Chang liver cells (Piao et al., 2011). In our system, using phase contrast inverted microscopy, AgNPs-treated cells were observed to have increased intracellular AgNPs concentrations compared to cells without AgNPs treatment. Consistent with our and other previous reports that nano-materials provoke oxidative stress (Harhaji et al., 2007; Limbach et al., 2007; Lin and Beal, 2006; Piao et al., 2011), our results showed that AgNPs induced ROS generation and cytotoxicity, which were significantly attenuated by an antioxidant NAC (Fig. 13). Cells are protected from the harmful effects of ROS by antioxidants such as SOD, CAT and GPx. SOD catalyzes the dismutation of superoxide radicals (a major form of ROS) into hydrogen peroxide, and CAT and GPx break down hydrogen peroxide into water (Betteridge, 2000; Fridovich, 1978; Halliwell, 1994; Robinson, 1998). In our study, we also found that AgNPs decreased the protein levels and activities of CAT and GPx (Fig. 13), which could lead to the increase in intracellular ROS levels and the induction of cell death. Previous reports indicated that the activation of the AMPK pathway reduced intracellular ROS levels (Kukidome et al., 2006; Li et al., 2009; Ouedraogo et al., 2006; Zhang et al., 2008). FOXO3 has recently been reported to be a direct target of AMPK, which phosphorylates FOXO3 to promote its activity (Greer et al., 2007a; Greer et al., 2007b).

In our system, AgNPs inhibited the active AMPK expression and led to the inhibition of active FOXO3 expression (Fig. 14). FOXO3 is involved in protection from oxidative stress by up-regulating CAT and GPx (Kojima et al., 2010; Nemoto and Finkel, 2002; Yalcin et al., 2008). It is noteworthy that AgNPs, which have been known to increase ROS levels and reduce ATP content in human cells (AshaRani et al., 2009), could not activate but rather inhibit AMPK pathway, which in turn could aggravate the oxidative cytotoxicity by downregulating antioxidant enzymes. Together with these findings, the differential modulation of cellular harmful effects of AgNPs by AMPK activator or inhibitor (Figs. 15 and 16) also supports the view that AgNPs might induce oxidative cytotoxicity by inhibiting the AMPK pathway. AICAR (an AMPK activator) decreased AgNPs-induced ROS levels and correspondingly, enhanced the CAT and GPx expression decreased by AgNPs, and recovered cell viability that was decreased by AgNPs. AICAR was supposed to possess direct antioxidant effect (Irrcher et al., 2009), and we also observed that AICAR could directly scavenge H_2O_2 in cell free system (data not shown), thus we hypothesized that AICAR prevented AgNPs-decreased enzymes activities and -induced toxicity maybe involve two mechanisms of action: (1) a direct scavenging effect on free radicals, and (2) an indirect effect via induction of AMPK activity. Conversely, Compound C (an AMPK inhibitor) enhanced AgNPs-induced ROS levels, and accordingly, further reduced the CAT and GPx expression and cell viability decreased by AgNPs. In addition, knockdown of AMPK by its specific siRNA markedly enhanced ROS generation and cytotoxicity. Thus, the up-regulation of the antioxidant system by the AMPK-FOXO3 signaling pathway may be an important protective mechanism against oxidative stress. Taken together, our data suggest that AgNPs inhibit AMPK signal pathway and down-regulate the phosphorylation of FOXO3. AgNPs induce the generation of ROS, and reduce antioxidant enzymes CAT and GPx via the inhibition of the AMPK-FOXO3 signaling pathway, and thereby induce cell death.

REFERENCES

Ahamed M, Alsalhi MS, Siddiqui MK. Silver nanoparticle applications and human health. Clin Chim Acta 2010b; 411:1841-8.

Ahamed M, Posgai R, Gorey TJ, Nielsen M, Hussain SM, Rowe JJ. Silver nanoparticles induced heat shock protein 70, oxidative stress and apoptosis in Drosophila melanogaster. Toxicol Appl Pharmacol 2010a;242: 263-9.

Amos S, Martin PM, Polar GA, Parsons SJ, Hussaini IM. Phorbol 12-myristate 13-acetate induces epidermal growth factor receptor transactivation via protein kinase Cdelta/c-src pathways in glioblastoma cells. J Biol Chem 2005;280:7729-38.

Anderson MF, Nilsson M, Eriksson PS, Sims NR. Glutathione monoethyl ester provides neuroprotection in a rat model of stroke. Neurosci Lett 2004;354:163-5.

Arora S, Jain J, Rajwade JM, Paknikar KM. Cellular responses induced by silver nanoparticles: In vitro studies. Toxicol Lett 2008;179:93-100.

Arora S, Jain J, Rajwade JM, Paknikar KM. Interactions of silver nanopar-ticles with primary mouse fibroblasts and liver cells. Toxicol Appl Pharmacol 2009;236:310-8.

AshaRani PV, Low Kah Mun G, Hande MP, Valiyaveettil S. Cytotoxicity and genotoxicity of silver nanoparticles in human cells. ACS Nano 2009;3:279-90.

Bartz RR, Suliman HB, Fu P, Welty-Wolf K, Carraway MS, MacGarvey NC, Withers CM, Sweeney TE, Piantadosi CA. Staphylococcus aureus sepsis and mitochondrial accrual of the 8-oxoguanine DNA glycosylase DNA repair enzyme in mice. Am J Respir Crit Care

Med 2011;183:226-33.

Baud O, Greene AE, Li J, Wang H, Volpe JJ, Rosenberg PA. Glutathione peroxidase-catalase cooperativity is required for resistance to hydrogen peroxide by mature rat oligodendrocytes. J Neurosci 2004;24:1531-40.

Bayet-Robert M, Loiseau D, Rio P, Demidem A, Barthomeuf C, Stepien G, Morvan D. Quantitative two-dimensional HRMAS 1H-NMR spectroscopy-based metabolite profiling of human cancer cell lines and response to chemotherapy. Magn Reson Med 2010;63: 1172-83.

Beauchamp MC, Letendre E, Renier G. 2002. Macrophage lipoprotein lipase expression is increased in patients with heterozygous familial hypercholesterolemia. J Lipid Res 2002;43:215-22.

Betteridge DJ. What is oxidative stress?. Metab Clin Exp 2000;49:3-8.

Boiteux S, Radicella JP. The human OGG1 gene: structure, functions, and its implication in the process of carcinogenesis. Arch Biochem Biophys 2000;377:1-8.

Bonfoco E, Krainc D, Ankarcrona M, Nicotera P, Lipton SA. Apoptosis and necrosis: Two distinct events induced, respectively, by mild and intense insults with N-methyl-D-aspartate or nitric oxide/superoxide in cortical cell cultures. Proc Natl Acad Sci U S A 1995;92:7162-6.

Briehl MM, Baker AF. Modulation of the antioxidant defence as a factor in apoptosis. Cell Death Differ 1996;3:63-70.

Carlson C, Hussain SM, Schrand AM, Braydich-Stolle LK, Hess KL, Jones RL, Schlager JJ,

Unique cellular interaction of silver nanoparticles: size-dependent generation of reactive oxygen species. J Phys Chem B 2008;112:13608-19.

Carmichael J, DeGraff WG, Gazdar AF, Minna JD, Mitchell JB. Evaluation of a tetrazolium-based semiautomated colorimetric assay: Assessment of chemosensitivity testing. Cancer Res 1987;47:936-42.

Carrillo MC, Kanai S, Nokubo M, Kitani K. (-) Deprenyl induces activities of both superoxide dismutase and catalase but not of glutathione peroxidase in the striatum of young male rats. Life Sci 1991;48:517-21.

Ceolotto G, Gallo A, Papparella I, Franco L, Murphy E, Iori E et al. Rosiglitazone reduces glucose-induced oxidative stress mediated by NAD(P)H oxidase via AMPK-dependent mechanism. Arterioscler Thromb Vasc Biol 2007;27;2627-33.

Chaloupka K, Malam Y, Seifalian AM. Nanosilver as a new generation of nanoproduct in biomedical applications. Trends Biotechnol 2010;28:580-8.

Chan EC, Koh PK, Mal M, Cheah PY, Eu KW, Backshall A, Cavill R, Nicholson JK, Keun HC, Metabolic profiling of human colorectal cancer using high-resolution magic angle spinning nuclear magnetic resonance (HR-MAS NMR) spectroscopy and gas chromatography mass spectrometry (GC/MS). J Proteome Res 2009;8:352-61.

Chan K, Han XD, Kan YW. An important function of Nrf2 in combating oxidative stress: detoxification of acetaminophen. Proc Natl Acad Sci USA 2001;98:4611-6.

Chang L, Karin M. Mammalian MAP kinase signalling cascades. Nature 2001;410:37-40.

Cheng D, Yang J, Zhao Y. Antibacterial materials of silver nanoparticles application in medical appliances and appliances for daily use. Chin Med Equip J 2004;4:26-32.

Cohen MS, Stern JM, Vanni AJ, Kelley RS, Baumgart E, Field D, Libertino JA, Summerhayes IC. In vitro analysis of a nanocrystalline silver-coated surgical mesh. Surg Infect (Larchmt) 2007;8:397-403.

Colombo SL, Moncada S. AMPKalpha1 regulates the antioxidant status of vascular endothelial cells. Biochem J 2009;421:163-9.

Cortes-Wanstreet MM, Giedzinski E, Limoli CL, Luderer U. Overexpression of glutamate-cysteine ligase protects human COV434 granulosa tumour cells against oxidative and gamma-radiation-induced cell death. Mutagenesis. 2009;24:211-24.

Cossarizza A, Baccarani-Contri M, Kalashnikova G, Franceschi C. A new method for the cytofluorimetric analysis of mitochondrial membrane potential using the J-aggregate forming lipophilic cation 5,5',6,6'-tetrachloro-1,1',3,3'-tetraethylbenzimidazolcarbocyanine iodide (JC-1). Biochem Biophys Res Commun 1993;197: 40-5.

Cox DP. Disruption of 8-hydroxy-2'-deoxyguanosine DNA glycosylase (Ogg1) antioxidant response capacity by sodium arsenite. Master's Thesis of The Uni-versity of Montana-Missoula 2007;39-91.

Czaja MJ. The future of GI and liver research: editorial perspectives III. JNK/AP-1 regulation of hepatocyte death. Am J Physiol Gastrointest Liver Physiol 2003;284:875-9.

Davis RJ. Signal transduction by the JNK group of MAP kinases. Cell 2000;103:239-52.

Denisova NA, Cantuti-Castelvetri I, Hassan WN, Paulson KE, Joseph JA. Role of membrane lipids in regulation of vulnerability to oxidative stress in PC12 cells: implication for aging. Free Radic Biol Med 2001;30:671-8.

de Souza-Pinto NC, Eide L, Hogue BA, Thybo T, Stevnsner T, Seeberg E, Klungland A, Bohr VA. Repair of 8-oxodeoxyguanosine lesions in mito-chondrial dna depends on the oxoguanine dna glycosylase (OGG1) gene and 8-oxoguanine accumulates in the mitochondrial dna of OGG1-defective mice. Cancer Res 2001;61:5378-81.

Dewanjee S, Maiti A, Sahu R, Dua TK, Mandal V. Effective Control of Type 2 Diabetes through Antioxidant Defense by Edible Fruits of Diospyros peregrina. Evid Based Complement Alternat Med 2009;7.

Dhénaut A, Boiteux S, Radicella JP. Characterization of the hOGG1 promoter and its expression during the cell cycle. Mutat Res 2000;461:109-18.

Díaz B, Sánchez-Espinel C, Arruebo M, Faro J, de Miguel E, Magadán S, Yagüe C, Fernández-Pacheco R, Ibarra MR, Santamaría J, González-Fernández A. Assessing methods for blood cell cytotoxic responses to inorganic nanoparticles and nanoparticle aggregates. Small 2008;4:2025-34.

Dinkova-Kostova AT, Holtzclaw WD, Cole RN, Itoh K, Wakabayashi N, Katoh Y, Yamamoto M, Talalay P. Direct evidence that sulfhydryl groups of Keap1 are the sensors regulating induction of phase 2 enzymes that protect against carcinogens and oxidants. Proc Natl Acad Sci USA 2002;99:11908-13.

Dizdaroglu M, Jaruga P, Birincioglu M, Rodriguez H. Free radical-induced damage to DNA: mechanisms and measurement. Free Radic Biol Med 2002;32:1102-15.

Dringen R, Pawlowski PG, Hirrlinger J. Peroxide detoxification by brain cells. J Neurosci Res 2005;79:157-65.

Eom HJ, Choi J. p38 MAPK activation, DNA damage, cell cycle arrest and apoptosis as mechanisms of toxicity of silver nanoparticles in jurkat T cells. Environ Sci Technol 2010;44:8337-42.

Ercal N, Gurer-Orhan H, Aykin-Burns N. Toxic metals and oxidative stress part I: mechanisms involved in metal-induced oxidative damage. Curr Top Med Chem 2001;1:529-39.

Foldbjerg R, Olesen P, Hougaard M, Dang DA, Hoffmann HJ, Autrup H. PVP-coated silver nanoparticles and silver ions induce reactive oxygen species, apoptosis and necrosis in THP-1 monocytes. Toxicol Lett 2009;190:156-62.

Fridovich I. The biology of oxygen radicals. Science 1978;201:875-80.

Fu J, Ji J, Fan, D, Shen J. Construction of antibacterial multilayer films containing nanosilver via layer-by-layer assembly of heparin and chitosan-silver ions complex. J Biomed Mater Res A 2006;79:665-74.

Gao N, Flynn DC, Zhang Z, Zhong XS, Walker V, Liu KJ, Shi X, Jiang BH. G1 cell cycle progression and the expression of G1 cyclins are regulated by PI3K/AKT/mTOR/p70S6K1 signaling in human ovarian cancer cells. Am J Physiol Cell Physiol 2004;287:C281-91.

Green DR, Reed JC. Mitochondria and apoptosis. Science 1998;281:1309-12.

Greer EL, Dowlatshahi D, Banko MR, Villen J, Hoang K, Blanchard D et al. An AMPK-FOXO pathway mediates longevity induced by a novel method of dietary restriction in C. elegans. Curr Biol 2007a;17:1646-56.

Greer EL, Oskoui PR, Banko MR, Maniar JM, Gygi MP, Gygi SP et al. The energy sensor AMP-activated protein kinase directly regulates the mammalian FOXO3 transcription factor. J Biol Chem 2007b;282:30107-19.

Habib GM, Shi ZZ, Lieberman MW. Glutathione protects cells against arsenite-induced toxicity. Free Radic Biol Med 2007;42:191-201.

Halliwell B, Aruoma OI. DNA damage by oxygen-derived species. Its mechanism and measurement in mammalian systems. FEBS Lett 1991;281:9-19.

Halliwell B. Free radicals, antioxidants, and human disease: Curiosity, cause, or consequence?. Lancet 1994;344:721-4.

Harhaji L, Isakovic A, Raicevic N, Markovic Z, Todorovic-Markovic B, Nikolic N et al. Multiple mechanisms underlying the anticancer action of nanocrystalline fullerene. Eur J Pharmacol 2007;568;89-98.

Hawkins CL, Davies MJ. Generation and propagation of radical reactions on proteins. Biochim Biophys Acta 2001;1504:196-219.

Hayashi T, Hirshman MF, Fujii N, Habinowski SA, Witters LA, Goodyear LJ. Metabolic stress and altered glucose transport: Activation of AMP-activated protein kinase as a unifying coupling mechanism. Diabetes 2000;49:527-31.

Herr I, Debatin KM. Cellular stress response and apoptosis in cancer therapy. Blood 2001;98:2603-14.

Hsin YH, Chen CF, Huang S, Shih TS, Lai PS, Chueh PJ. The apoptotic effect of nanosilver is mediated by a ROS- and JNK-dependent mechanism involving the mitochondrial pathway in NIH3T3 cells. Toxicol Lett 2008;179:130-9.

Hussain SM, Hess KL, Gearhart JM, Geiss KT, Schlager JJ. In vitro toxicity of nanoparticles in BRL 3A rat liver cells. Toxicol In Vitro 2005;19:975-83.

Hyun JW, Choi JY, Zeng HH, Lee YS, Kim HS, Yoon SH, Chung MH. Leukemic cell line, KG-1 has a functional loss of hOGG1 enzyme due to a point mutation and 8-hydroxydeoxyguanosine can kill KG-1. Oncogene 2000;19:4476-9.

Hyun JW, Jung YC, Kim HS, Choi EY, Kim JE, Yoon BH, Yoon SH, Lee YS, Choi J, You HJ, Chung MH. 8-Hydroxydeoxyguanosine causes death of human leukemia cells deficient in 8-oxoguanine glycosylase 1 activity by inducing apoptosis. Mol Cancer Res 2003;1:290-9.

Ido Y, Carling D, Ruderman N. Hyperglycemia-induced apoptosis in human umbilical vein endothelial cells: Inhibition by the AMP-activated protein kinase activation. Diabetes 2002;51:159-67.

Irrcher I, Ljubiclc V, Hood DA. Interactions between ROS and AMP kinase activity in the regulation of PGC-1α transcription in skeletal muscle cells. Am J Physiol Cell Physiol 2009:296;C116-23.

Itoh K, Tong KI, Yamamoto M. Molecular mechanism activating Nrf2-Keap1 pathway in regulation of adaptive response to electrophiles. Free Radic Biol Med 2004;36:1208-13.

Itoh K, Wakabayashi N, Katoh Y, Ishii T, Igarashi K, Engel JD, Yamamoto M. Keap1 represses nuclear activation of antioxidant responsive elements by Nrf2 through binding to the amino-terminal Neh2 domain. Genes Dev 1999;13:76-86.

Jo M, Park MH, Choi DY, Yuk DY, Lee YM, Lee JM, Jeong JH, Oh KW, Lee MS, Han SB, Hong JT. Neuroprotective Effect of L-Theanine on Aß-Induced Neurotoxicity through Anti-Oxidative Mechanisms in SK-N-SH and SK-N-MC Cells. Biomol Ther 2011;19:288-95.

Johnston HJ, Hutchison G, Christensen FM, Peters S, Hankin S, Stone V. A review of the in vivo and in vitro toxicity of silver and gold particulates: Particle attributes and biological mechanisms responsible for the observed toxicity. Crit Rev Toxicol 2010;40:328-46.

Kamata H, Honda S, Maeda S, Chang L, Hirata H, Karin M. Reactive oxygen species promote TNFalpha-induced death and sustained JNK activation by inhibiting MAP kinase phosphatases. Cell 2005;120:649-61.

Kandel ES, Skeen J, Majewski N, Di Cristofano A, Pandolfi PP, Feliciano CS, Gartel A, Hay N. Activation of Akt/protein kinase B overcomes a G(2)/m cell cycle checkpoint induced by DNA damage. Mol Cell Biol 2002;22:7831-41.

Kannan S, Pang H, Foster DC, Rao Z, Wu M. Human 8-oxoguanine DNA glycosylase increases resistance to hyperoxic cytotoxicity in lung epithelial cells and involvement with altered MAPK activity. Cell Death Differ 2006;13:311-23.

Kim S, Choi JE, Choi J, Chung KH, Park K, Yi J, Ryu DY. Oxidative stress-dependent toxicity of silver nanoparticles in human hepatoma cells. Toxicol In Vitro 2009;23:1076-84.

Kim YC, Masutani H, Yamaguchi Y, Itoh K, Yamamoto M, Yodoi J. Hemininduced activation of the thioredoxin gene by Nrf2. A differential regulation of the antioxidant responsive element by a switch of its binding factors. J Biol Chem 2001;276:18399-406.

Klungland A, Rosewell I, Hollenbach S, Larsen E, Daly G, Epe B, Seeberg E, Lindahl T, Barnes DE. Accumulation of premutagenic DNA lesions in mice defective in removal of oxidative base damage. Proc Natl Acad Sci USA 1999;96:13300-5.

Kojima T, Norose T, Tsuchiya K, Sakamoto K. Mouse 3T3-L1 cells acquire resistance against oxidative stress as the adipocytes differentiate via the transcription factor FoxO. Apoptosis 2010;15:83-93.

Kreuter J, Gelperina S. Use of nanoparticles for cerebral cancer. Tumori 2008;94:271-7.

Kroemer G, Zamzami N, Susin SA. Mitochondrial control of apoptosis. Immunol Today 1997;18:44-51.

Kukidome D, Nishikawa T, Sonoda K, Imoto K, Fujisawa K, Yano M et al. Activation of AMP-activated protein kinase reduces hyperglycemia-induced mitochondrial reactive oxygen species production and promotes mitochondrial biogenesis in human umbilical vein endothelial cells. Diabetes 2006;55:120-7.

Kwak MK, Itoh K, Yamamoto M, Kensler TW. Enhanced expression of the transcription factor Nrf2 by cancer chemopreventive agents: role of antioxidant response element-like sequences in the nrf2 promoter. Mol Cell Biol 2002;22:2883-92.

Lee HY, Park HK, Lee YM, Kim K, Park SB. A practical procedure for producing silver nanocoated fabric and its antibacterial evaluation for biomedical applications. Chem

Commun (Camb) 2007;28:2959-61.

Lee JM, Johnson JA. An important role of Nrf2-ARE pathway in the cellular defense mechanism. J Biochem Mol Biol 2004;37:139-43.

Lewinski N, Colvin V, Drezek R. Cytotoxicity of nanoparticles. Small 2008;4:26-49.

Li MH, Jang JH, Na HK, Cha YN, Surh YJ. Carbon monoxide produced by heme oxygenase-1 in response to nitrosative stress induces expression of glutamatecysteine ligase in PC12 cells via activation of phosphatidylinositol 3- kinase and Nrf2 signaling. J Biol Chem 2007;282:28577-86.

Li P, Nijhawan D, Budihardjo I, Srinivasula SM, Ahmad M, Alnemri ES, Wang X. Cytochrome c and dATP-dependent formation of Apaf-1/caspase-9 complex initiates an apoptotic protease cascade. Cell 1997;91:479-89.

Li XN, Song J, Zhang L, LeMaire SA, Hou X, Zhang C et al. Activation of the AMPK-FOXO3 pathway reduces fatty acid-induced increase in intracellular reactive oxygen species by upregulating thioredoxin. Diabetes 2009;58:2246-57.

Liddell JR, Dringen R, Crack PJ, Robinson SR. Glutathione peroxidase 1 and a high cellular glutathione concentration are essential for effective organic hydroperoxide detoxification in astrocytes. Glia 2006;54:873-9.

Limbach LK, Wick P, Manser P, Grass RN, Bruinink A, Stark WJ. Exposure of engineered nanoparticles to human lung epithelial cells: influence of chemical composition and catalytic activity on oxidative stress. Environ Sci Technol 2007;41:4158-63.

Lin A. Activation of the JNK signaling pathway: breaking the brake on apoptosis. Bioessays 2003;25:17-24.

Lin MT, Beal MF. Mitochondrial dysfunction and oxidative stress in neurodegenerative diseases. Nature 2006;443;787-95.

Liu X, Kim CN, Yang J, Jemmerson R, Wang X. Induction of apoptotic program in cell-free extracts: requirement for dATP and cytochrome c. Cell 1996;86:147-57.

Luoma SN. Silver Nanotechnologies and the Environment: Old Problems or New Challenges. The Pew Charitable Trusts and the Woodrow Wilson International Center for Scholars. 2008.

Madamanchi NR, Runge MS. Mitochondrial dysfunction in atherosclerosis. Circ Res 2007;100:460-73.

Manzer R, Wang J, Nishina K, McConville G, Mason RJ. Alveolar epithelial cells secrete chemokines in response to IL-1beta and lipopolysaccharide but not to ozone. Am J Respir Cell Mol Biol 2006;34:158-66.

Mao X, Yu CR, Li WH, Li WX. Induction of apoptosis by shikonin through a ROS/JNK-mediated process in Bcr/Abl-positive chronic myelogenous leukemia (CML) cells. Cell Res 2008;18:879-88.

Marinkovic D, Zhang X, Yalcin S, Luciano JP, Brugnara C, Huber T et al. Foxo3 is required for the regulation of oxidative stress in erythropoiesis. J Clin Invest 2007;117:2133-44.

Martindale JL, Holbrook NJ. Cellular response to oxidative stress: signaling for suicide and survival. J Cell Physiol 2002;192:1-15.

Merrill CL, Ni H, Yoon LW, Tirmenstein MA, Narayanan P, Benavides GR, Easton MJ, Creech DR, Hu CX, McFarland DC, Hahn LM, Thomas HC, Morgan KT. Etomoxir-induced oxidative stress in HepG2 cells detected by differential gene expression is confirmed biochemically. Toxicol Sci 2002;68:93-101.

Moi P, Chan K, Asunis I, Cao A, Kan YW. Isolation of NF-E2-related factor 2 (Nrf2), a NF-E2-like basic leucine zipper transcriptional activator that binds to the tandem NF-E2/AP1 repeat of the beta-globin locus control region. Proc Natl Acad Sci USA 1994;91:9926-30.

Morel Y, Barouki R. Repression of gene expression by oxidative stress. Biochem J 1999;342 Pt 3:481-96.

Nel A, Xia T, Mädler L, Li N. Toxic potential of materials at the nanolevel. Science 2006;311:622-7.

Nemoto S, Finkel T. Redox regulation of forkhead proteins through a p66shc-dependent signaling pathway. Science 2002;295:2450-2.

Nguyen T, Sherratt PJ, Huang HC, Yang CS, Pickett CB. Increased protein stability as a mechanism that enhances Nrf2-mediated transcriptional activation of the antioxidant response element. Degradation of Nrf2 by the 26 S proteasome. J Biol Chem 2003;278:4536-41.

Nguyen T, Yang CS, Pickett CB. The pathways and molecular mechanisms regulating Nrf2 activation in response to chemical stress. Free Radic Biol Med 2004;37:433-41.

Nicoletti I, Migliorati G, Pagliacci MC, Grignani F, Riccardi C. A rapid and simple method for measuring thymocyte apoptosis by propidium iodide staining and flow cytometry. J Immunol Methods 1991;139:271-9.

Nicotera P, Ankarcrona M, Bonfoco E, Orrenius S, Lipton SA. Neuronal necrosis and apoptosis: Two distinct events induced by exposure to glutamate or oxidative stress. Adv Neurol 1997;72:95-101.

Okimotoa Y, Watanabea A, Nikia E, Yamashitab T, Noguchia N. A novel fluorescent probe diphenyl-1-pyrenylphosphine to follow lipid peroxidation in cell membranes. FEBS Lett 2000;474:137-40.

Ouedraogo R, Wu X, Xu SQ, Fuchsel L, Motoshima H, Mahadev K et al. Adiponectin suppression of high-glucose-induced reactive oxygen species in vascular endothelial cells: Evidence for involvement of a cAMP signaling pathway. Diabetes 2006;55:1840-6.

Paglia DE, Valentine WN. Studies on the quantitative and qualitative characterization of erythrocyte glutathione peroxidase. J Lab Clin Med 1967;70:158-69.

Papaiahgari S, Kleeberger SR, Cho HY, Kalvakolanu DV, Reddy SP. NADPH oxidase and ERK signaling regulates hyperoxia-induced Nrf2-ARE transcriptional response in pulmonary epithelial cells. J Biol Chem 2004;279:42302-12.

Peña-Llopis S, Ferrando MD, Peña JB. Fish tolerance to organophosphate-induced oxidative stress is dependent on the glutathione metabolism and enhanced by N-acetylcysteine. Aquat Toxicol 2003;65:337-60.

Piantadosi CA, Carraway MS, Babiker A, Suliman HB. Heme oxygenase- 1 regulates cardiac

mitochondrial biogenesis via Nrf2-mediated transcriptional control of nuclear respiratory factor-1. Circ Res 2008;103:1232-40.

Piao MJ, Kang KA, Lee IK, Kim HS, Kim S, Choi JY et al. Silver nanoparticles induce oxidative cell damage in human liver cells through inhibition of reduced glutathione and induction of mitochondria-involved apoptosis. Toxicol Lett 2011;201:92-100.

Rajagopalan R, Ranjan SK, Nair CK. Effect of vinblastine sulfate on gamma-radiation-induced DNA single-strand breaks in murine tissues. Mutat Res 2003;536:15-25.

Robinson BH. The role of manganese superoxide dismutase in health and disease. J Inherit Metab Dis 1998;21:598-603.

Rosenkranz AR, Schmaldienst S, Stuhlmeier KM, Chen W, Knapp W, Zlabinger GJ. A microplate assay for the detection of oxidative products using 2',7'-dichlorofluorescin-diacetate. J Immunol Methods 1992;156:39-45.

Santos SC, Lacronique V, Bouchaert I, Monni R, Bernard O, Gisselbrecht S, Gouilleux F. Constitutively active STAT5 variants induce growth and survival of hematopoietic cells through a PI 3-kinase/Akt dependent pathway. Oncogene 2001;20:2080-90.

Sastre J, Pallardó FV, Viña J. Mitochondrial oxidative stress plays a key role in aging and apoptosis. IUBMB Life 2000;49:427-35.

Shaulian E, Karin M. AP-1 as a regulator of cell life and death. Nat Cell Biol 2002;4:E131-6.

Shen HM, Liu ZG. JNK signaling pathway is a key modulator in cell death mediated by reactive oxygen and nitrogen species. Free Radic Biol Med 2006;40:928-39.

Shiba D, Shimamoto N. Attenuation of endogenous oxidative stress-induced cell death by cytochrome P450 inhibitors in primary cultures of rat hepatocytes. Free Radic Biol Med 1999;27:1019-26.

Shim JH, Cho KJ, Lee KA, Kim SH, Myung PK, Choe YK et al. E7-expressing HaCaT keratinocyte cells are resistant to oxidative stress-induced cell death via the induction of catalase. Proteomics 2005;5:2112-22.

Shin SM, Kim SG. Inhibition of arachidonic acid and iron-induced mitochondrial dysfunction and apoptosis by oltipraz and novel 1,2-dithiole-3-thione congeners. Mol Pharmacol 2009;75:242-53.

Shtarkman IN, Gudkov SV, Chernikov AV, Bruskov VI. Effect of amino acids on X-ray-induced hydrogen peroxide and hydroxyl radical formation in water and 8-oxoguanine in DNA. Biochemistry 2008;73:470-8.

Sies H. Glutathione and its role in cellular functions. Free Radic Biol Med 1999;27:916-21.

Singh NP. Microgels for estimation of DNA strand breaks, DNA protein crosslinks and apoptosis. Mutat Res 2000;455:111-27.

Srivastava RK, Mi QS, Hardwick JM, Longo DL. Deletion of the loop region of Bcl-2 completely blocks paclitaxel-induced apoptosis. Proc Natl Acad Sci USA 1999;96:3775-80.

Sroka IC, Nagle RB, Bowden GT. Membrane-type 1 matrix metalloproteinase is regulated by sp1 through the differential activation of AKT, JNK, and ERK pathways in human prostate tumor cells. Neoplasia 2007;9:406-17.

Stadtman ER. Oxidation of free amino acids and amino acid residues in proteins by radiolysis and by metal-catalyzed reactions. Annu Rev Biochem 1993;62:797-821.

Struthers L, Patel R, Clark J, Thomas S. Direct detection of 8-oxodeoxyguanosine and 8-oxoguanine by avidin and its analogues. Anal Biochem 1998;255:20-31.

Su J, Zhang J, Liu L, Huang Y, Mason RP. Exploring feasibility of multicolored CdTe quantum dots for in vitro and in vivo fluorescent imaging. J Nanosci Nanotechnol 2008;8:1174-7.

Tan WB, Jiang S, Zhang Y. Quantum-dot based nanoparticles for targeted silencing of HER2/neu gene via RNA interference. Biomaterials 2007;28:1565-71.

Tauskela JS, Hewitt K, Kang LP, Comas T, Gendron T, Hakim A, Hogan M, Durkin J, Morley P. Evaluation of glutathione-sensitive fluorescent dyes in cortical culture. Glia 2000;30:329-41.

Terai K, Hiramoto Y, Masaki M, Sugiyama S, Kuroda T, Hori M et al. AMP-activated protein kinase protects cardiomyocytes against hypoxic injury through attenuation of endoplasmic reticulum stress. Mol Cell Biol 2005;25:9554-75.

Toyokuni S. Reactive oxygen species-induced molecular damage and its application in pathology. Pathol Int 1999;49:91-102.

Tsuruya K, Furuichi M, Tominaga Y, Shinozaki M, Tokumoto M, Yoshimitsu T, Fukuda K, Kanai H, Hirakata H, Iida M, Nakabeppu Y. Accumulation of 8-oxoguanine in the cellular DNA and the alteration of the OGG1 expression during ischemia-reperfusion injury in the rat kidney. DNA Repair 2003;2:211-29.

Tsuzuki T, Nakatsu Y, Nakabeppu Y. Significance of error-avoiding mechanisms for oxidative DNA damage in carcinogenesis. Cancer Sci 2007;98:465-70.

Ueta E, Sasabe E, Yang Z, Osaki T, Yamamoto T. Enhancement of apoptotic damage of squamous cell carcinoma cells by inhibition of the mitochondrial DNA repairing system. Cancer Sci 2008;99:2230-7.

Vadim I, Lyudmila V, Zhaksylyk K, Anatoly V. Heat-induced formation of reactive oxygen species and 8-oxoguanine, a biomarker of damage to DNA. Nucleic Acids Res 2002;30:1354-63.

Vairetti M, Griffini P, Pietrocola G, Richelmi P, Freitas I. Cold-induced apoptosis in isolated rat hepatocytes: protective role of glutathione. Free Radic Biol Med 2001;31:954-61.

Venugopal R, Jaiswal AK. Nrf2 and Nrf1 in association with Jun proteins regulate antioxidant response element-mediated expression and coordinated induction of genes encoding detoxifying enzymes. Oncogene 1998;17:3145-56.

Vigneshwaran N, Kathe AA, Varadarajan PV, Nachane RP, Balasubramanya RH. Functional finishing of cotton fabrics using silver nanoparticles. J Nanosci Nanotechnol 2007;7:1893-7.

Wang L, Chen Y, Sternberg P, Cai J. Essential roles of the PI3 kinase/Akt pathway in regulating Nrf2-dependent antioxidant functions in the RPE. Invest Ophthalmol Vis Sci 2008;49:1671-8.

Wanzel M, Kleine-Kohlbrecher D, Herold S, Hock A, Berns K, Park J, Hemmings B, Eilers M. Akt and 14-3-3eta regulate Miz1 to control cell-cycle arrest after DNA damage. Nat Cell Biol 2005;7:30-41.

Xu X, Yang Q, Bai J, Lu T, Li Y, Jing X. Fabrication of biodegradable electrospun poly (L-lactide-co-glycolide) fibers with antimicrobial nanosilver particles. J Nanosci Nanotechnol 2008;8:5066-70.

Yalcin S, Zhang X, Luciano JP, Mungamuri SK, Marinkovic D, Vercherat C et al. Foxo3 is essential for the regulation of ataxia telangiectasia mutated and oxidative stress-mediated homeostasis of hematopoietic stem cells. J Biol Chem 2008;283:25692-705.

Yang J, Liu X, Bhalla K, Kim CN, Ibrado AM, Cai J, Peng TI, Jones DP, Wang X. Prevention of apoptosis by Bcl-2: release of cytochrome c from mitochondria blocked. Science 1997;275:1129-32.

Yoon KY, Hoon Byeon J, Park JH, Hwang J. Susceptibility constants of Escherichia coli and Bacillus subtilis to silver and copper nanoparticles. Sci Total Environ 2007;373:572-5.

Yu C, Rahmani M, Dai Y, Conrad D, Krystal G, Dent P, Grant S. The lethal effects of pharmacological cyclin-dependent kinase inhibitors in human leukemia cells proceed through a phosphatidylinositol 3-kinase/Akt-dependent process. Cancer Res 2003;63:1822-33.

Yun H, Kim HS, Lee S, Kang I, Kim SS, Choe W et al. AMP kinase signaling determines whether c-jun N-terminal kinase promotes survival or apoptosis during glucose deprivation. Carcinogenesis 2009;30:529-37.

Zamzami N, Marchetti P, Castedo M, Hirsch T, Susin SA, Masse B, Kroemer G. Inhibitors of permeability transition interfere with the disruption of the mitochondrial transmembrane potential during apoptosis. FEBS Lett 1996;384:53-7.

Zamzami N, Marchetti P, Castedo M, Zanin C, Vayssiere JL, Petit PX, Kroemer G. Reduction in mitochondrial potential constitutes an early irreversible step of programmed lymphocyte death in vivo. J Exp Med 1995;181:1661-72.

Zhang M, Dong Y, Xu J, Xie Z, Wu Y, Song P et al. Thromboxane receptor activates the AMP-activated protein kinase in vascular smooth muscle cells via hydrogen peroxide. Circ Res 2008;102:328-37.

Zhivotovsky B, Orrenius S, Brustugus OT, Doskeland SO. Injected cytochrome c induces apoptosis. Nature 1998;391:449-50.

Zimmerman JJ. Redox/radical repertoire rapport: pathophysiology and therapeutics. Acta Anaesthesiol Scand 1998;42:1-3.

Zipper LM, Mulcahy RT. Erk activation is required for Nrf2 nuclear localization during pyrrolidine dithiocarbamate induction of glutamate cysteine ligase modulatory gene expression in HepG2 cells. Toxicol Sci 2003;73:124-34.

Zou H, Henzel WJ, Liu X, Lutschg A, Wang X. Apaf-1, a human protein homologous to C. elegans CED-4, participates in cytochrome c-dependent activation of caspase-3. Cell 1997;90:405-13.

ABSTRACT IN KOREAN

은나노 입자 제품중에서 항균특성을 이용한 제품들이 많은데 이중에서 여러가지 의학용품과 일상용품들을 많이 볼수가 있다.

은나노 입자 제품들이 널리 사용되고 있지만 은나노 입자에 노출 후 세포독성작용에 대한 연구는 아직 적은것으로 알려져 있다. 이 연구는 은나노 입자의 세포독성작용에 관한 분자적 메커니즘을 조사하였다.

우선, 은나노 입자로 인한 세포독성이 은 이온 소스인 질산은과 비교하여 훨씬 높다는 것을 보여주었다. 인간의 정상 간세포인 Chang 세포에서 은나노 입자는 환원형 글루타치온의 억제작용을 통하여 활성산소종을 생성한다. 은나노 입자에 의해 생성되는 활성산소종은 세포내 성분을 손상시키는데 DNA 절단, 지질막 과산화작용, 단백질 카보닐화작용을 유도한다. 은나노 입자에 노출 후 아폽토시스, 예를 들면 아폽토틱 바디의 형성, sub-G_1 hypodiploid 세포, DNA 분열 등을 통해 세포 생존율이 감소된다. Bax, Bcl-2 발현의 조절을 통한 은나노 입자로 유도되는 미토콘드리아 의존적인 아폽토틱 경로는 미토콘드리아 막전위의 붕괴를 유도한다. 미토콘드리아 막전위의 손실은 미토콘드리아로부터 cytochrome C를 방출하여 caspase 9와 caspase 3을 활성화시킨다. 은나노 입자의 아폽토틱 작용은 JNK의 활성화 그리고 JNK 억제제인 SP600125와 JNK 타깃 siRNA에 의한 억제를 통해 약화된다.

8-Oxoguanine (8-oxoG)은 활성산소종으로 유도되는 DNA 손상에 민감한 마커이다. 8-Oxoguanine DNA glycosylase 1 (OGG1)은 중요한 DNA 수복 효소로서 8-oxoG을 인지하고 절단한다. 은나노 입자로 유도되는 산화적 스트레스가 OGG1에 대한 작용과 은나노 입자에 의한 세포독성 메커니즘을 밝히기 위해 아래 단계 연구를 수행하였다. 은나노 입자가 OGG1 mRNA와 단백질 발현을 감소하여 OGG1 활성을 약화시켜서 8-oxoG 레벨을 증가시킨다. 전사인자인 Nrf2는 중요한 인자로서

OGG1의 조절작용을 유도한다. 은나노 입자는 핵내 Nrf2 발현, 핵내로의 이동, Nrf2의 전사활성을 감소시킨다. ERK와 AKT는 Nrf2의 상위로서 OGG1의 발현을 돕는다. 은나노 입자는 ERK와 AKT 단백질 발현의 활성화 폼을 감소시켜서 Nrf2의 억제작용과 OGG1 발현의 감소를 유도한다.

CAT나 GPx와 같은 항산화 효소는 산화적 스트레스로부터 직접적으로 세포를 보호한다고 보고되었다. 마지막 연구는 인간 간세포인 Chang 세포에서 은나노 입자에 의한 세포 내 높은 량의 ROS 레벨에 있어서 항산화제의 역할과 분자적인 메커니즘을 조사하였다.

은나노 입자는 ROS 레벨을 증가시키는 동시에 CAT와 GPx의 발현과 활성, 그리고 세포생존율을 감소하지만 강력한 항산화제인 NAC에 의해 확연하게 ROS 레벨을 감소하고 CAT와 GPx의 활성을 회복시키며 세포사멸을 완화한다. 은나노는 AMP-activated protein kinase (AMPK)-forkhead transcription factor 3 (FOXO3) 경로를 감소시키는데 이는 항산화 효소의 유발을 위한 신호경로이다. AMPK 활성화제인 AICAR는 확연하게 CAT와 GPx의 발현을 회복시키며 ROS 레벨과 세포독성을 감소시키지만 AMPK 억제제인 Compound C는 이와 상반된 변화를 관측하였다.

결론적으로 이 연구는 은나노 입자로 유도되는 세포독성이 산화적 스트레스에 의한 아폽토시스와 세포내 성분의 손상에 의한 것이다. 또 은나노 입자의 노출은 ERK와 AKT의 비활성화 작용을 통하여 Nrf2로 매개되는 OGG1을 하류 조절한다는 것을 증명하였다. 은나노 입자로 유도되는 산화적 세포독성은 적어도 부분적인 원인은 AMPK-FOXO3 경로의 억제작용을 거쳐 항산화 효소의 활성을 감소시킨다는 것을 알려주었다.

감사의 글

유학 온지가 엊그제 같은데 벌써 6년이란 세월이 흘러서 졸업을 맞게 되었네요. 그동안 너무나도 부족한 저에게 많은 도움을 주신 고마운 분들께 감사의 마음을 전하고 싶습니다.

석사 학위를 받은 후 취직을 해야 할지 공부를 계속 해야 할지 갈피를 잡지 못해 망설이고 있을 때 지도교수님이신 현진원 교수님께서 저에게 많은 조언을 해주시고 한단계 더 높은 박사 공부를 할 수 있는 소중한 기회를 주신 덕분에 오늘날 결실을 맺을 수 있게 되었습니다. 교수님의 따뜻한 관심과 배려 속에서 6년의 시간도 눈 깜짝할 사이에 지나간 것 같습니다. 진심으로 감사 드립니다. 그리고 연구와 강의로 항상 바쁘신 가운데에도 저의 학위 논문 심사를 흔쾌히 맡아주시고 많은 조언을 해주신 박덕배 교수님, 강희경 교수님, 유은숙 교수님께 진심으로 감사의 마음 전합니다. 또한 바쁜 와중에도 멀리 육지에서 제주도까지 내려오신 인하대 박헌주 교수님께도 진심으로 감사 드립니다. 그리고 학업으로 쌓이는 스트레스를 풀 수 있도록 항상 유머와 호탕한 웃음으로 즐거움을 선사하시는 조문제 교수님, 날카로운 지적과 합리적인 조언을 잊지 않으시는 고영상 교수님, 언제나 상냥한 웃음으로 맞아주시고 관심과 배려를 아끼지 않으시는 은수용 교수님을 비롯하여 가르침을 주신 모든 교수님들께도 감사의 마음을 전하고 싶습니다.

적지 않은 나이에도 불구하고 학업을 다시 시작할 수 있게 도와준 친구 미화, 넌 내게 인생의 전환점을 맞게 해주었어. 고마운 마음 평생 간직하며 보답할게.

경아와 장예, 나이는 나보다 어리지만 선배답게 공부, 실험, 생활 할 것 없이 항상 많은 것을 알려주고 챙겨줘서 6년동안 정말 든든했다. 내 얕팍한 단어지식으로서는 감사한 마음 표현할 수가 없구나. 기천이와 아름이, 선배인 내가

준 것은 없고 너희들께 받기만 한 것 같구나. 그동안 너희 둘이 있어서 참 많이 의지가 됐었어. 항상 고맙게 생각하고 있다. 그리고 유재, 영민이, 정언이도 후배로 와줘서 반갑고 또 잘 따라줘서 너무 고맙다.

같은 실험실에 있는 영미씨, 박사 동기로 들어와서 같이 졸업하게 되니 더더욱 반갑고 또 지금까지 보여준 많은 관심과 도움은 정말 잊을 수 없을꺼예요. 그리고 한때는 같은 실험실에서 같이 일하던 희경, 진영, 지은, 창희씨께도 감사의 마음 전합니다.

가까운 이웃나라이지만 문화 정서상 결코 같지만은 않은 서먹한 이 땅에서 만나 동고동락하면서 지내온 연희와 금희, 지강이, 관건, 너희들과 같이 있어서 6년이란 세월을 외롭지 않게 보낸것 같다. 그리고 중국에서도 항상 잊지 않고 안부 물어보는 선매, 연옥이, 홍렬이, 군학이, ... 그 외 관심을 보여준 친구들 다들 너무너무 고맙다.

마지막으로 저를 낳아주시고 헌신적으로 길러주신 우리 엄마, 언제나 진심어린 격려와 아낌없는 도움을 주는 든든한 내 동생, 그리고 시어머니께 효도하는 사랑스럽고 심성 착한 우리 올케, 가족들한테는 항상 미안한 마음과 고마운 마음을 함께 느끼게 되네요. 졸업의 기쁨을 중국에 있는 가족들과 한국에서 돈 버느라 고생하시면서도 공부하는 저를 잊지 않고 챙겨주신 여러 친지들과 함께 나누고 싶습니다. 그리고 생전에 꼭 박사까지 공부하라고 하시던 아버지, 하늘나라에서라도 무지 기뻐하실 우리 아버지께 이 작은 결실을 바칩니다.

이 외에도 미처 언급하지 못한 고마운 분들이 너무나도 많습니다만 이름을 하나하나 되새기지 못함을 죄송하게 생각하며 모든 분들께 감사의 마음 전하고 싶습니다.